Chapter 9

KLYSTRONS

We have seen in Chapter 7 the deleterious effects that occur in conventional triodes and tetrodes as the signal frequency is increased. The factors degrading gain-bandwidth product and power output in these tubes may be divided into two categories:

1. *Circuit Factors*
   These include lead inductance, stray capacitance, and power losses due to radiation, dielectric loss factor, and resistance.

2. *Transit-Time Effects*
   These effects occur because of the finite time electrons take to travel between electrodes.

The losses due to circuit factors can be reduced by a judicious use of the microwave components discussed in the preceding chapter. On the other hand, one encounters certain fundamental difficulties in trying to minimize transit-time effects. In the triode and the tetrode, it is the cathode-to-grid transit time which is the real culprit degrading the high-frequency gain and efficiency. One can decrease this transit time by decreasing the cathode-to-grid spacing. This approach has been used successfully in the Western Electric 416B triode, described in Section 7.4. But as one can see from the dimensions of this tube, as given in Section 7.4, it is unlikely that the operating frequency could be extended much higher by further reduction of electrode spacings. Accordingly, one must seek other means for modulating the electron beams in tubes operating at high microwave frequencies.

In the present chapter we shall describe two microwave tubes which make use of a second type of modulation called *velocity modulation*. Velocity modulation is obtained by impressing a small ac component of velocity

on a dc electron beam. This can be done by allowing the beam to pass through two grids between which there is applied a small ac voltage. If the grids are spaced very close together, equal numbers of electrons emerge from the grids in equal intervals of time, but the velocity of the electrons has a small ac component. Such a beam is said to be velocity modulated. As the electrons travel away from the grids, the faster electrons move away from the slower electrons behind them and tend to overtake the slower electrons ahead of them. The axial density of electrons is therefore no longer uniform, and the beam current passing a point some distance from the grids has an ac component. In view of this, it is frequently said that the velocity modulation imparted to the beam when it passed through the grids gives rise to current modulation farther along the beam.

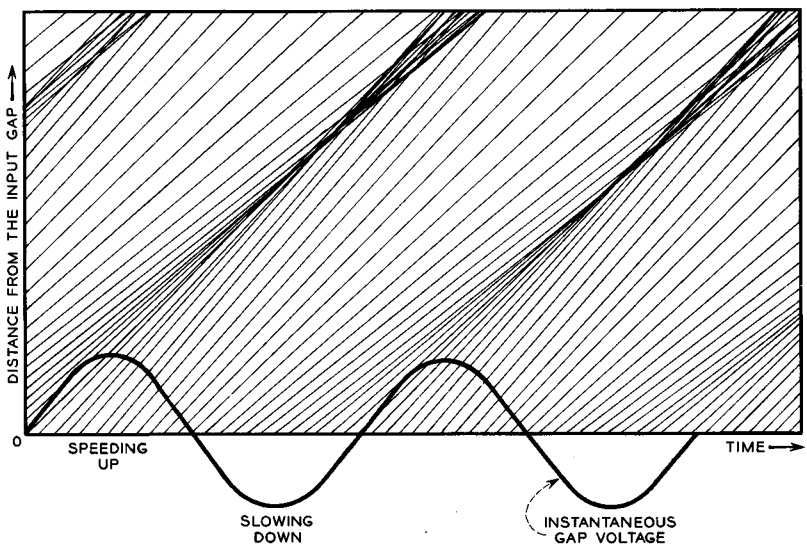

FIG. 9-1 Applegate diagram showing representative electron trajectories. The slope of each trajectory is proportional to the electron velocity. Velocity modulation is produced at the gap by the changing gap voltage. This results in density modulation beyond the gap.

The velocity modulation is illustrated in Figure 9-1, known as an Applegate diagram. In this figure, plots of distance vs. time are given for a number of representative electrons (24 per cycle). The effects of space-charge forces are neglected in drawing the figure. The electrons leave the grids spaced uniformly in time, corresponding to the lack of current modulation at this point, However, each electron has a slightly different velocity,

depending on the instantaneous rf voltage between the grids when the electron passed through the grids. The instantaneous voltage between the grids is indicated on the figure. The slope of a trajectory is proportional to the electron velocity. Because of the difference in slopes, many of the trajectories converge so as to form electron bunches at some distance from the grids. We note that the bunches tend to form about an electron which goes through the grids when the voltage is zero and increasing. Similarly, the electrons tend to move away from an electron which goes through the grids when the voltage is zero and decreasing; this electron locates what is termed the antibunch.

If the ac voltage applied between the grids is of a very high frequency, the distance along the beam between maxima and minima in velocity will, of course, be very short. This means that appreciable density variations

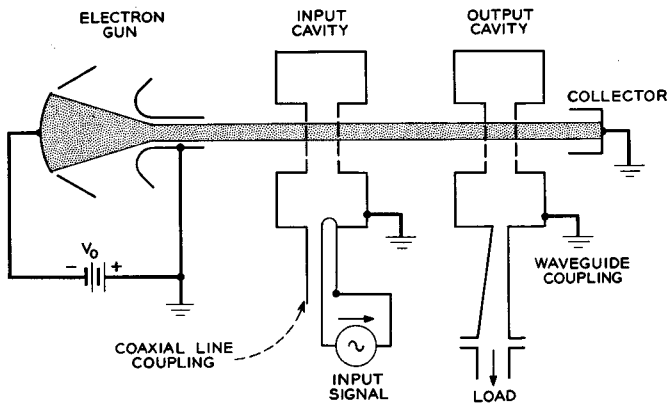

FIG. 9-2 Two-cavity klystron amplifier.

will appear after the electrons have traveled a relatively short distance from the grids. Velocity modulation, therefore, lends itself particularly to high-frequency tubes. The two velocity modulated tubes described in the present chapter, the klystron amplifier and the reflex oscillator, are generally designed for operation at frequencies above 200 Mc. Reflex klystron oscillators have been built which give useful output at frequencies greater than 100,000 Mc, or 100 Gc.

In both these tube types the beam passes through grids that are an integral part of a resonant cavity. If the cavity is excited, the voltage developed across the cavity, and hence between the grids, imparts the velocity modulation to the beam. Power is extracted from the beam in the case of the klystron amplifier by allowing the beam to pass through a second resonant cavity. The cavity is excited by the induced currents associated

with the beam just as in the case of an external resonant circuit connected between a pair of grids. In the reflex oscillator the beam is caused to return through the modulating cavity with the right phase so that it adds to the excitation energy of the cavity.

Figure 9-2 illustrates a two-cavity klystron amplifier. In this particular example the rf signal is coupled into the input cavity by means of a coaxial cable. The output cavity is coupled to the load by means of a waveguide, taking advantage of the lower attenuation inherent in waveguide.

The electron beam is produced by an electron gun of the type shown in Figure 4.5-1(a). This is a convergent Pierce gun which produces a small diameter beam from a cathode of much larger diameter. Thus, much higher beam current densities are available for a given cathode electron-emission density than in a triode or tetrode. This allows a large increase in the beam power passing through electrode gaps of a fixed area and capacitance and hence a large increase in the gain-bandwidth product which can be achieved with such a tube. The klystron is usually operated with the cathode at a negative potential and the other electrodes grounded, for reasons of convenience and safety.

Since the electrons must travel a considerable distance, the beam is prevented from spreading radially, due to the space charge repulsion, by applying an axial dc magnetic field. This field is provided by a permanent magnet or solenoid, as discussed in Section 3.4.

After passing through the output cavity, the beam strikes a collector electrode. The function of the collector electrode could be performed by replacing the second grid of the output cavity with a solid piece of metal. However, having a separate electron collector has several advantages. First, the collector can be made as large as is desired in order to collect the beam at a lower power density, thus minimizing localized heating. If the collector were part of the rf circuit, its size would be limited by the maximum gap capacitance consistent with good high-frequency performance. Second, by having a separate collector, its potential can be reduced considerably below the beam potential in the rf interaction region, thus reducing the power dissipated in the collector and increasing the overall efficiency of the device. It should be clear that the electron beam does not extract energy from any dc power supply unless the electrons are actually collected by an electrode connected to that power supply. Thus in Figure 9-2, if a separate power supply were connected between cathode and collector and if the cavity grids intercepted a negligible part of the beam, the power supply between the cathode and collector would be the only one supplying any power to the tube.

It is clear that the two-cavity klystron amplifier has considerable advantage over the conventional triode and tetrode for microwave signal ampli-

fication. Circuit losses are greatly reduced by the use of resonant cavities at the interaction gaps and by the use of microwave transmission lines for making input and output connections. Furthermore, transit-time effects, which limit the high-frequency performance of triodes and tetrodes, are largely overcome by the use of velocity modulation. In the following sections, we shall take a more quantitative look at the electron interaction process in the klystron amplifier. Later in the chapter we shall describe the reflex klystron oscillator.

9.1 Quantitative Theory of Klystron Interaction

The quantitative theory of klystron interaction may be conveniently divided into three parts, as follows:

1. The velocity modulation produced by a given voltage at the input cavity.
2. The current modulation at the output cavity resulting from the initial velocity modulation at the input cavity.
3. The current induced in the output cavity by the current modulation on the beam.

The first and third parts have to do with the interaction between an electron beam and the grids of a cavity. (The region between the grids of a cavity is known as the cavity gap.)

(a) *Velocity Modulation Produced by an RF Voltage Applied to the Grids of a Cavity*

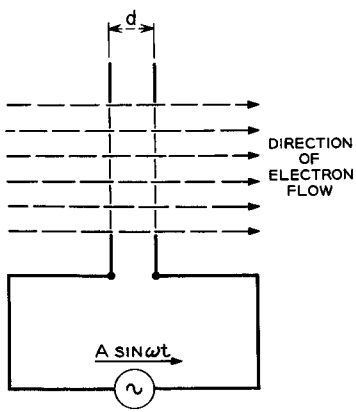

FIG. 9.1-1 Klystron buncher gap with rf voltage applied. Velocity modulation is produced on the electron beam.

The grids of the input cavity are represented in the equivalent circuit of Figure 9.1-1. An rf voltage source is shown connected to these grids. This voltage source is an equivalent source at the grids which replaces the external signal source indicated in Figure 9-2. As indicated in the introduction, this voltage will produce a velocity modulation on the beam, whose value we shall now determine.

Let the z axis be taken in the direction of electron flow, with the entrance grid at the position $z = 0$. The grids are assumed to be ideal; that is, all electrons pass through

without interception, and the rf electric field lines are perpendicular to and terminate on the grids.

Although an electron is between the grids, it experiences a force due to the rf electric field. This force causes an acceleration, as in Equation (1.1-1).

$$\frac{d^2z}{dt^2} = -\frac{e}{m}E_z \tag{9.1-1}$$

This equation holds for time-varying electric fields as well as for static fields. For the gap in Figure 9.1-1,

$$E_z = -\frac{A}{d}\sin \omega t \tag{9.1-2}$$

where d is the grid spacing, and $A \sin \omega t$ is the instantaneous gap voltage. Thus, the motion of an electron is given by the solution to the equation:

$$\frac{d^2z}{dt^2} = \frac{eA}{md}\sin \omega t \tag{9.1-3}$$

Integrating once, we obtain

$$\frac{dz}{dt} = u_o - \frac{eA}{\omega md}(\cos \omega t - \cos \omega t_1) \tag{9.1-4}$$

where t_1 is the time at which the electron passed through the first grid, and u_o is the dc velocity of the electrons entering the gap. The velocity u_o is given by

$$u_o = \sqrt{\frac{2e}{m}V_o} \tag{9.1-5}$$

where V_o is the dc voltage of the electron beam, as in Figure 9-2. Equation (9.1-4) gives the velocity of the electron at any instant while it is in the gap. To find the exit velocity, we must substitute the time at which the electron leaves the gap for t in the above equation. Calling this time t_2, the exit velocity is given by

$$u(d) = u_o - \frac{eA}{\omega md}(\cos \omega t_2 - \cos \omega t_1) \tag{9.1-6}$$

If we assume that the amplitude of the rf voltage A is very small compared with the dc voltage of the beam V_o, the electron transit time in the gap is very nearly that given by the dc velocity alone. Thus, if t_o is the instant at which the electron is at the center of the gap,

$$t_1 = t_o - \frac{d}{2u_o} \tag{9.1-7}$$

and

$$t_2 = t_o + \frac{d}{2u_o} \tag{9.1-8}$$

If these expressions are substituted into Equation (9.1-6) and if we simplify the resulting expression by the use of trigonometric identities, we obtain the following expression for the exit velocity:

$$u(d) = u_o + \frac{2eA}{\omega md} \sin \frac{\omega d}{2u_o} \sin \omega t_o \tag{9.1-9}$$

If the beam-coupling coefficient M is defined as in Chapter 7,

$$M = \frac{\sin \dfrac{\omega d}{2u_o}}{\dfrac{\omega d}{2u_o}} \tag{9.1-10}$$

Equation (9.1-9) becomes

$$\begin{aligned} u(d) &= u_o + \frac{eMA}{mu_o} \sin \omega t_o \\ &= u_o\left(1 + \frac{MA}{2V_o} \sin \omega t_o\right) \end{aligned} \tag{9.1-11}$$

M is plotted as a function of the gap transit time in Figure 7.1-2. It is unity for zero transit time and drops off for non-zero values of transit time.

(*b*) *The Bunching Process*

Having discussed the process by which velocity modulation is produced on the beam at the input gap, we next consider the mechanism by which this velocity modulation causes bunching or current modulation to occur in the drift region between the two cavities.

This bunching process has already been described in connection with Figure 9-1, and we shall now seek a quantitative description of the process in order to answer important questions such as: What should the spacing be between the two cavities in order to achieve a maximum degree of bunching? What magnitude of current is induced in the output cavity?

For the moment we shall neglect the mutually repulsive forces of space charge. This approximation is reasonably valid for low-power tubes, where the electron density in the beam is relatively small. We shall further assume that all motion is in the z direction. Physically, this requires either that the space-charge forces be too small to cause transverse spreading or else that the electron motion be confined by a strong dc magnetic field in the z direction.

The electrons emerging from the input cavity have a velocity given by Equation (9.1-11). Since there are no accelerating fields in the drift space between the two cavities, each electron moves at a constant velocity given

by this equation for its particular value of t_o. This behavior has been depicted in the Applegate diagram of Figure 9-1.

Assuming a separation l between the centers of the input and output cavity gaps, the time of arrival t of a particular electron at the output cavity is given by the expression:

$$t - t_o = \frac{l}{u_o\left(1 + \frac{M}{2}\frac{A}{V_o}\sin \omega t_o\right)} \tag{9.1-12}$$

Let us make the simplifying assumption that the input cavity voltage amplitude is much less than the dc beam voltage. This will be true in most cases, except for some very high power tubes. The second term in the

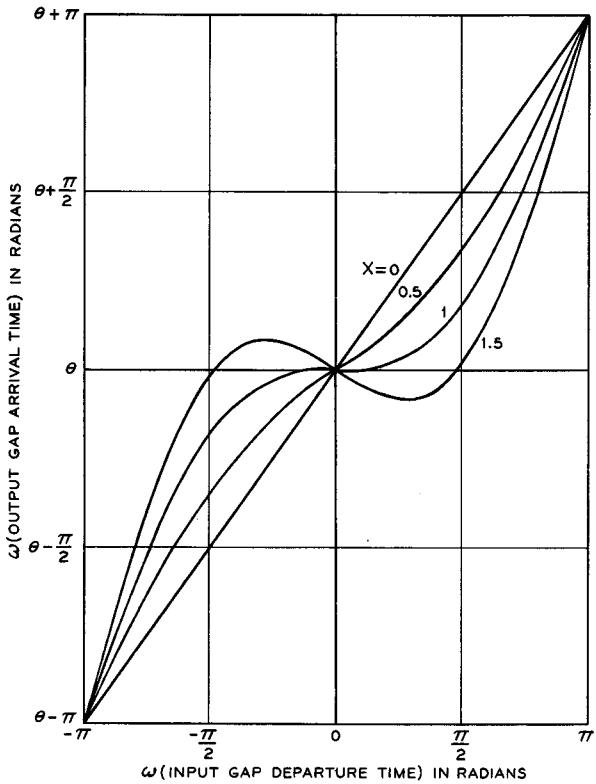

FIG. 9.1-2 Output-gap arrival time plotted vs. the time of departure from the input gap for various values of X, the bunching parameter, defined by Equation (9.1-14). θ is the dc transit angle. For X greater than unity, some electrons leaving the input gap at three different instants arrive at the same instant at the output gap.

denominator is thus much less than unity, and Equation (9.1-12) can be approximately written as

$$t - t_o = \frac{l}{u_o}\left(1 - \frac{M}{2}\frac{A}{V_o}\sin \omega t_o\right) \tag{9.1-13}$$

or, in terms of radians,

$$\begin{aligned}\omega t - \omega t_o &= \theta\left(1 - \frac{M}{2}\frac{A}{V_o}\sin \omega t_o\right) \\ &= \theta - X \sin \omega t_o \end{aligned} \tag{9.1-14}$$

where $\theta = \omega l/u_o$ is the dc transit angle between cavities, and $X = (M/2)(A/V_o)\theta$ is a parameter known as the bunching parameter.

In Figure 9.1-2 are plotted curves showing output-gap arrival time as a function of input-gap departure time over one rf cycle, for various values of the bunching parameter. One notes that for values of the bunching parameter greater than unity, the departure time is a multivalued function of the arrival time for electrons near the bunch center. However, the arrival time is always a single-valued function of the departure time.

Let us first consider the situation for X less than unity. The instantaneous current reaching the output cavity can be written as

$$i(t) = \frac{dq}{dt} \tag{9.1-15}$$

where dq is the amount of charge arriving at the output cavity in a time interval dt. In Figure 9.1-2 the ordinate and abscissa are proportional to t and t_o, respectively. We see from this figure that the amount of charge arriving in a time dt can be related to the corresponding departure time interval dt_o by

$$dq = -I_o dt_o \tag{9.1-16}$$

since electrons leave the input cavity evenly spaced at a rate given by the dc current. The minus sign is used so that I_o may be a positive quantity; dq is of course negative for electrons.

Substituting Equation (9.1-16) into Equation (9.1-15), we obtain

$$i(t) = -I_o\frac{dt_o}{dt} \tag{9.1-17}$$

where the derivative is obtained simply by measuring slopes on the curve of Figure 9.1-2. Current waveforms for several values of the bunching parameter are shown in Figure 9.1-3. Infinite current peaks are obtained at the arrival times for which the curves of Figure 9.1-2 have zero slope.

For values of the bunching parameter greater than unity, the fact that the curve of Figure 9.1-2 is multivalued results in three values of slope for a

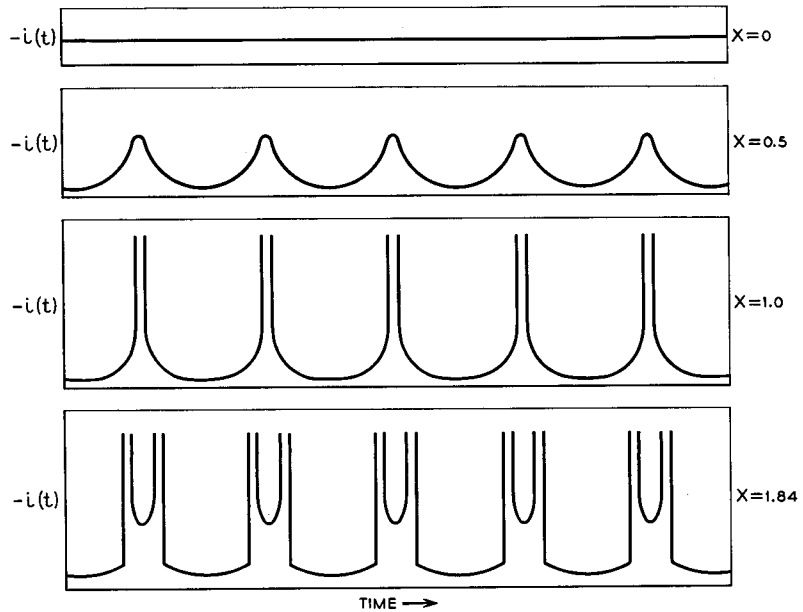

FIG. 9.1-3 Beam current waveforms at the output gap. For X greater than or equal to unity, infinite peaks are obtained at the points corresponding to zero slope in Figure 9.1-2. In an actual tube, these peaks though large would remain finite because of the space-charge forces.

given arrival time near the bunch center. This situation is easily handled as follows. Since Equation (9.1-16) must include the total charge for a given arrival time, we must include a term for each of the three departure times; thus

$$dq = -I_o [dt_o|_1 + dt_o|_2 + dt_o|_3] \tag{9.1-18}$$

Corresponding to Equation (9.1-17), we obtain

$$i(t) = -I_o \left[\left| \frac{dt_o}{dt} \right|_1 + \left| \frac{dt_o}{dt} \right|_2 + \left| \frac{dt_o}{dt} \right|_3 \right] \tag{9.1-19}$$

In each case, the absolute value of the derivative must be taken. Physically this corresponds to the fact that the charge increment dq has the same sign regardless of the sequence of arrival of the electrons. A negative value of dt_o/dt merely indicates that electrons which left the input cavity last arrive at the output cavity first; dq always has a negative value.

The current waveforms of Figure 9.1-3 may be Fourier analyzed to determine the fundamental component and the various harmonics. This

could be done graphically. However, it is possible to solve this problem analytically. We shall proceed with such an analysis.

The current at the output gap can be written as the Fourier series:

$$i(t) = -I_o + \sum_{n=1}^{\infty} [a_n \cos n(\omega t - \theta) + b_n \sin n(\omega t - \theta)] \quad (9.1\text{-}20)$$

where

$$a_n = \frac{1}{\pi} \int_{\theta-\pi}^{\theta+\pi} i(t) \cos n(\omega t - \theta) d(\omega t)$$

and

$$b_n = \frac{1}{\pi} \int_{\theta-\pi}^{\theta+\pi} i(t) \sin n(\omega t - \theta) d(\omega t)$$

Let us consider first the situation for X less than unity, so that the curves of Figure 9.1-2 are single-valued.

It will be convenient to change the variable of integration from arrival time to departure time. Equation (9.1-17) gives us

$$i(t)d(\omega t) = -I_o d(\omega t_o) \quad (9.1\text{-}21)$$

From Figure 9.1-2, we see that the limits of integration become $-\pi$ to $+\pi$. When Equations (9.1-21) and (9.1-14) are substituted into the above integrals, we obtain

$$a_n = -\frac{I_o}{\pi} \int_{-\pi}^{\pi} \cos n(\omega t_o - X \sin \omega t_o) d(\omega t_o)$$

and

$$b_n = -\frac{I_o}{\pi} \int_{-\pi}^{\pi} \sin n(\omega t_o - X \sin \omega t_o) d(\omega t_o) \quad (9.1\text{-}22)$$

b_n is identically equal to zero since the integrand is an odd function of ωt_o. The definite integral in the expression for a_n is given by a Bessel function:[1]

$$2J_n(nX) = \frac{1}{\pi} \int_{-\pi}^{\pi} \cos n(\omega t_o - X \sin \omega t_o) d(\omega t_o) \quad (9.1\text{-}23)$$

Equation (9.1-20) thus becomes

$$i(t) = -I_o - 2I_o \sum_{n=1}^{\infty} J_n(nX) \cos n(\omega t - \theta) \quad (9.1\text{-}24)$$

For values of X greater than unity, the same expression is obtained. This is shown in Appendix XV. For small values of X, $J_1(X) \approx X/2$ and $J_n(nX)$

[1]Reference 9.1, p. 150.

is very small for $n > 1$. Equation (9.1-24) then becomes $i(t) = -I_o$ $[1 + X \cos(\omega t - \theta)]$ for small X and hence for small input signals.

Equation (9.1-24) shows that the various harmonics in the bunched beam have amplitudes proportional to Bessel functions of order n, where n is the

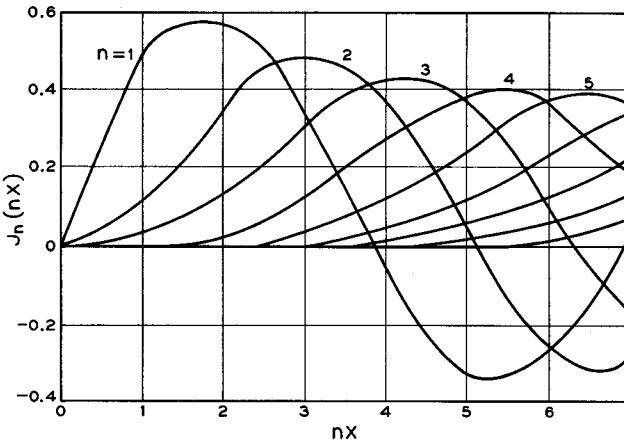

FIG. 9.1-4 Bessel functions of various orders. The maximum value of J_1 occurs at $X = 1.84$ and is equal to 0.582.

same as the harmonic. These Bessel functions are plotted in Figure 9.1-4. Since the abscissa in this figure is proportional to the transit time between cavities, we can adjust either the beam velocity or the distance between cavities so as to obtain a maximum amplitude for any of the harmonics. For an amplifier, we would make X equal to 1.84 so as to peak the fundamental component at the output cavity. On the other hand, it is also possible to use the tube of Figure 9-2 as a harmonic generator, in which case we would choose the transit time to correspond to the peak of one of the higher-order Bessel functions of Figure 9.1-4. Since these other peaks are nearly as large as that of the fundamental, the two-cavity klystron can be a very efficient harmonic generator. Of course, the output cavity would be tuned to the harmonic frequency.

Since the electrons become bunched about an electron which passed through the input cavity when the voltage across the input cavity was changing from decelerating the electrons to accelerating them, the center of the electron bunch arrives at the output cavity delayed by the dc transit angle, but advanced by $\pi/2$. This can also be seen by comparison of the phase of the voltage applied to the input cavity with the phase of the fundamental component in Equation (9.1-24).

(c) *Current Induced in the Output Cavity by the Bunched Beam*

To complete the description of klystron interaction, we must consider the current induced in the output cavity by the bunched beam. This problem has already been considered in Section 7.1(a), where we have considered the current induced by a modulated beam into a load connected between two grids. Although the discussion presented in Chapter 7 was applied to a tetrode, it might equally well be applied to a klystron, where we interpret the pair of grids to be the grids of a re-entrant cavity resonator.

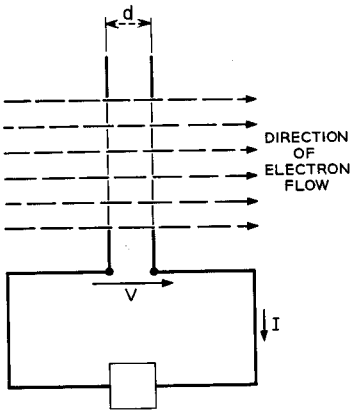

FIG. 9.1-5 Convention for positive induced current adopted in this chapter. The induced current is equal to M times the beam current modulation at the center of the gap (in magnitude and phase).

We shall find it convenient to adopt the conventions for positive gap voltage and induced current indicated in Figure 9.1-5. The direction for positive induced current is opposite to that used in Chapters 6 and 7. In microwave tube work it is customary to assume that the ac component of beam current is positive when directed from left to right. Thus, the induced current indicated in Figure 9.1-5 is positive when the ac component of beam current is positive.

From Equation (9.1-24), the dc and fundamental components of beam current at the output cavity are given by

$$i(l,t) = -I_o + i_1 \cos \omega\left(t - \frac{l}{u_o}\right) \tag{9.1-25}$$

where

$$i_1 = -2I_o J_1(X) \tag{9.1-26}$$

and we have substituted $\theta = \omega l/u_o$. But this is exactly the same type of wavelike behavior that was assumed for the beam current density in Section 7.1(a). From Section 7.1(a), therefore, we have the result that the induced current (with positive direction assumed as in Figure 9.1-5) is given by $M_2 i_1 \cos \omega(t - l/u_o)$, or in phasor notation we may write:

$$I = M_2 i_1 \epsilon^{-j(\omega/u_o)l} \tag{9.1-27}$$

where I and $i_1\epsilon^{-j(\omega/u_o)l}$ are phasor quantities representing the induced current and the fundamental component of beam current at the gap center,

respectively. M_2 is the beam-coupling coefficient for the output cavity. Simply stated, the induced current is M_2 times the fundamental component of the beam current at the gap center, both in magnitude and in phase.

This is really a very important result; the induced current is independent of the loading of the output cavity. Thus, the modulated beam truly acts

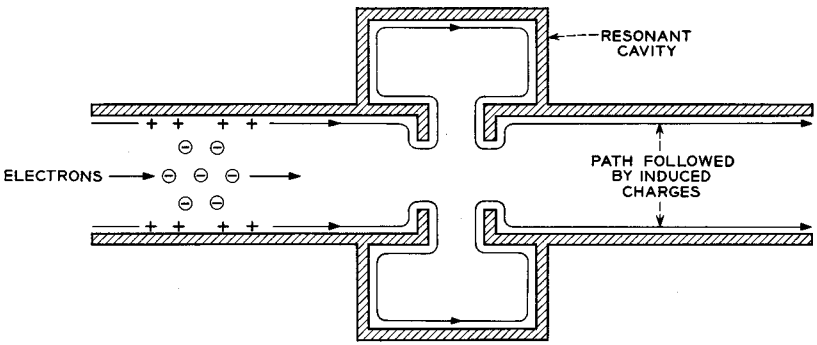

FIG. 9.1-6 Path followed by the induced charges associated with an electron bunch passing through a cavity.

as a current source. Figure 9.1-6 shows the path followed by the induced charges associated with a single bunch of electrons which passes through the output cavity.

At resonance the phase of the oscillations in the output cavity is such that maximum decelerating voltage appears across the output cavity when maximum number of electrons is crossing the gap. This follows from the fact that at resonance the cavity and load appear as a resistance connected between the grids, so that when the induced current reaches a maximum, the voltage across the cavity is also a maximum. This explains the transfer of energy from the beam to the cavity.

How much power can be delivered to the output cavity and load from the bunched beam? This question can be answered most easily from a consideration of the equivalent circuit of the output cavity, shown in Figure 9.1-7.

In this equivalent circuit, L and C are the inductance and capacitance of the re-entrant cavity itself, without the presence of the beam. These parameters are obtained as discussed in the introduction to Chapter 8. Similarly G_c is a conductance which accounts for the resistive and dielectric losses in the cavity. These parameters determine the *cold* unloaded Q of the cavity, defined by

$$Q_o = \frac{\omega_c C}{G_c} \tag{9.1-28}$$

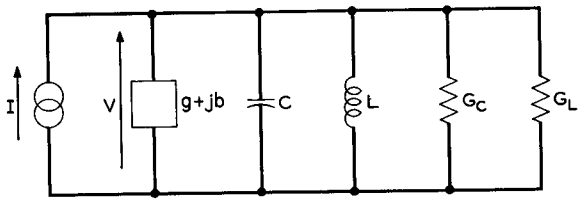

FIG. 9.1-7 Equivalent circuit for the output cavity and its load. The symbols used are defined as follows:

V = gap voltage
I = induced current
C = gap capacitance
L = cavity inductance
$g + jb$ = beam loading admittance
G_c = conductance representing cavity losses
G_L = load conductance (as seen from the cavity gap)

where ω_c is the cavity resonant frequency in radians.

The beam-loading admittance is given by $g + jb$. The parameters g and b are functions of the gap transit time. For an unmodulated beam, they are given by Equations (7.1-14) and plotted in Figure 7.1-4. Physically, these parameters express the fact that for a non-zero gap transit time, some energy is exchanged between the electrons and the rf energy stored in the output cavity. It is convenient to assume the same parameters for a modulated beam. This is a small-signal approximation, useful in predicting the small-signal performance of a klystron amplifier.

In most practical tubes, the output gap transit angle is much less than π, and the susceptive component is capacitive, as shown in Figure 7.1-4. Furthermore, when the transit angle is much less than π, b varies linearly with frequency, and we may write

$$b = \omega C_b \tag{9.1-29}$$

where $C_b = g_o T_o/12$. Here g_o and T_o are defined as in Equation (7.1-14). The *hot* unloaded Q is defined by

$$Q_u = \frac{\omega_o(C + C_b)}{G_c + g} \tag{9.1-30}$$

where ω_o is the resonant frequency of the cavity with the beam present. Q_u thus includes the intrinsic cavity parameters plus the loading due to the electron beam. It should be noted that for the small-signal approximation we are considering, Q_u is independent of whether or not the beam is velocity modulated in the input cavity. Thus it could be evaluated by measuring

the characteristics of the output cavity with the beam turned on, but with no rf drive on the input cavity.[2]

In Figure 9.1-7 the conductance G_L accounts for the load connected to the cavity. Since the actual load will be separated from the cavity by waveguide, transformers, and various other components, G_L is an effective value as seen at the cavity gap. It is defined so as to give a correct value for the power absorbed for any given gap voltage. The external Q is defined by

$$Q_e = \frac{\omega_o(C + C_b)}{G_L} \tag{9.1-31}$$

The loaded Q is the Q of the whole circuit of Figure 9.1-7. It is thus given by

$$Q_l = \frac{\omega_o(C + C_b)}{G_c + g + G_L} \tag{9.1-32}$$

From the last three equations, we note that

$$\frac{1}{Q_l} = \frac{1}{Q_u} + \frac{1}{Q_e} \tag{9.1-33}$$

The remaining parameters in Figure 9.1-7 are the gap voltage V and the induced current I, defined previously.

To deliver maximum power to the load, we adjust the parameters such that

$$G_L = G_c + g \tag{9.1-34}$$

and

$$\omega^2 L(C + C_b) = 1 \tag{9.1-35}$$

Equation (9.1-34) may also be stated as

$$Q_e = Q_u \tag{9.1-36}$$

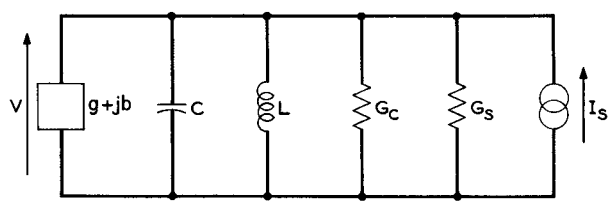

FIG. 9.1-8 Equivalent circuit for the input cavity and the signal source. The symbols used are as defined in Figure 9.1-7, with the additions:

I_s = current source representing the rf input signal

G_s = source conductance (as seen from the cavity gap)

[2]Measurements of resonant cavity characteristics are discussed in Reference 9.2.

The load conductance may be adjusted by changing the coupling of the cavity to the load. The resonance condition, Equation (9.1-35), may be obtained by varying the cavity capacitance or inductance. One common way to do this is to deform mechanically the cavity to change the gap spacing, thus changing the cavity capacitance.

The equivalent circuit for the input cavity is shown in Figure 9.1-8. Here the current source at the right represents the rf input source. The other parameters have the same meaning as in Figure 9.1-7, except that G_L is replaced by G_s, the source conductance.

9.2 Reflex Klystrons

The klystron amplifier of Figure 9-2 is an extremely stable type of microwave tube, where stability refers to freedom from oscillations. In normal operation there is no feedback from the output cavity to the input cavity, except perhaps by secondary electrons produced at or beyond the output cavity which make their way back to the input cavity. In order to make this tube oscillate, it is necessary to provide an external feedback path from the output cavity to the input cavity. This can be accomplished by tapping off a portion of the output power and feeding it back into the input cavity by means of an external transmission line. The oscillation frequency and power output are then determined by the simultaneous requirement that the loop gain be unity and the loop phase shift be a multiple of 2π radians. The loop phase shift can be varied by changing either the beam voltage or the length of the feedback cable. Of course, if the frequency is varied any appreciable amount, the cavities must be retuned.

For many applications of microwave oscillators, it is necessary to change the frequency rapidly. This is most readily done if the oscillation frequency can be varied electronically. In the oscillator described above, this can be done over a limited frequency range by changing the beam voltage. However, varying the beam voltage simultaneously varies the beam power, and this results in a larger change in output power with frequency than is desirable for most applications. This drawback is eliminated in the reflex klystron described below.

A schematic drawing of the reflex klystron, together with the power supply connections, is shown in Figure 9.2-1(a). A potential profile along the electron beam is shown in Figure 9.2-1(b). The electron gun injects the electron beam through the grids of a re-entrant microwave cavity. The electrons then approach an electrode known as the repeller, which is at a lower potential than the cathode. The repelling electric field in this region causes the electrons to "turn around" and pass once again through the cavity grids, but in the opposite direction. The electrons are then collected

on the walls of the cavity or other grounded metal parts of the tube. Since this tube is a relatively low-power device, the power dissipated in the cavity by the incident electrons is not excessive. The broken lines in Figure 9.2-1

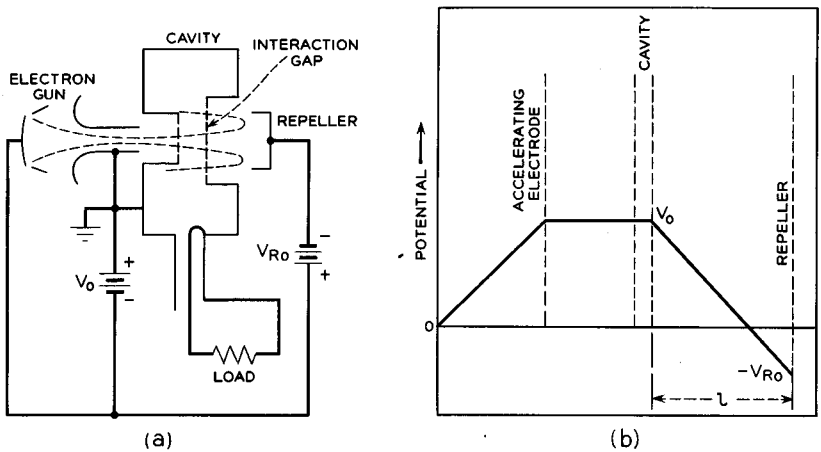

FIG. 9.2-1 Reflex klystron and its potential profile. (a) Schematic drawing of the tube showing the power supply connections. (b) Potential profile along the beam from the cathode to the repeller.

indicate the trajectories of the outermost electrons in the beam. The reflex klystron is usually operated without any magnetic field to confine the beam, and consequently the beam spreads under the influence of its own space charge. However, since the total distance traveled by the electrons is small, the total radial spreading is not excessive.

If we postulate an rf voltage on the cavity grids, the beam is velocity modulated during its first passage through the grids. While the electrons are in the repeller region, the velocity modulation is converted into current modulation, much like in the drift space between cavities of a klystron amplifier. When the current modulated beam re-enters the cavity, it induces an rf current in the walls of the cavity, as in the output cavity of the amplifier. This induced current is then the source of output power. The gap voltage is also produced by this induced current. Hence, the cavity serves a dual purpose; it is both the input cavity and the output cavity with feedback intrinsically provided.

The bunching mechanism in the repeller region can best be described by means of the Applegate diagram given in Figure 9.2-2(a). The corresponding gap voltage as a function of time is shown in Figure 9.2-2(b). Time markers are included on the abscissa in Figure 9.2-2(a), marking the

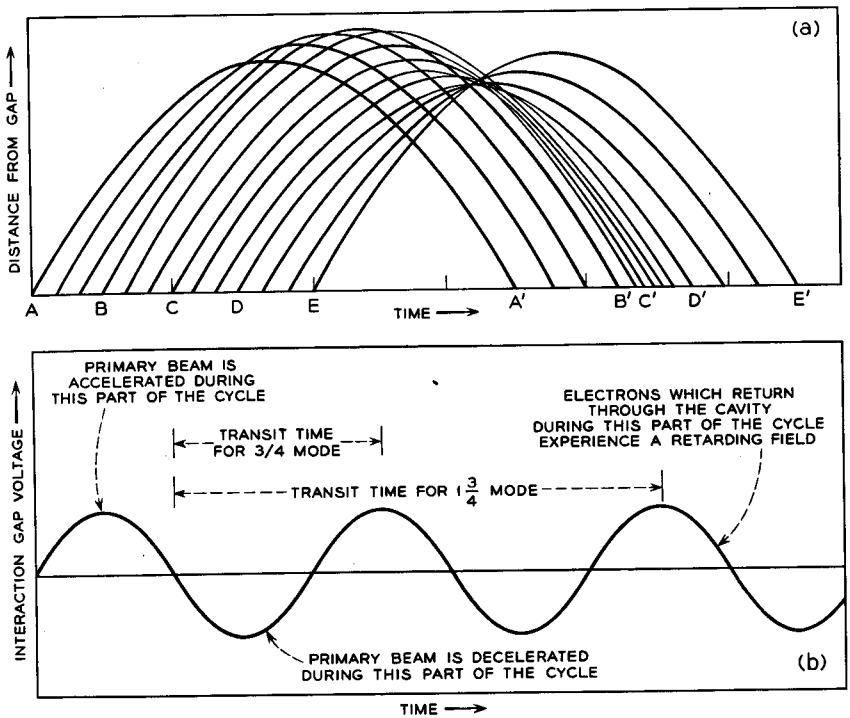

FIG. 9.2-2 Electron trajectories in a reflex klystron showing the dependence on the instantaneous gap voltage at the moment of departure. (a) Applegate diagram for the $1\frac{3}{4}$ mode of oscillation. (b) Instantaneous gap voltage.

instants for which the gap voltage is zero. Figure 9.2-2(a) shows distance-time plots for several electrons passing through the cavity at equally spaced intervals during one cycle of the cavity voltage. The electrons start out toward the repeller, are "turned around," and arrive back at the gap at a later time. Each electron leaves the gap with a different velocity, depending on the instantaneous value of the gap voltage as it passes through. Electron B passes through when the voltage is a maximum, and it receives the greatest increment of velocity. It therefore penetrates farthest toward the repeller before being turned back. On the other hand, electron D passes through when the gap voltage is maximally retarding, thus penetrating the least distance and arriving back in the shortest time span. Electrons A, C, and E go through the gap when the voltage is zero and penetrate toward the repeller an intermediate distance.

We note that a bunch forms around electron C which initially passed through the gap when the voltage was zero and decreasing. Since the bunch

arrives back at the gap at such an instant that the voltage is maximally retarding, energy is transferred from the beam to the cavity. In the diagram shown, eight of the electrons are slowed down in their second transit through the cavity, whereas only four are speeded up.

Since the dc transit time in the repeller region corresponds to $1\frac{3}{4}$ rf cycles for the condition shown in Figure 9.2-2, this mode of oscillation is known as the $1\frac{3}{4}$ mode. Alternatively, a higher magnitude of reflector voltage would cause the electrons all to return to the gap in a shorter span of time, and oscillation in the $\frac{3}{4}$ mode is possible. This occurs when the dc transit time corresponds to $\frac{3}{4}$ of an rf cycle. It is not necessary to have the transit time exactly $\frac{3}{4}$ or $1\frac{3}{4}$ cycles; oscillations are possible for slight departures from these values, but at reduced power levels and at slightly different frequencies. It is only necessary that the bunch be so phased that sufficient energy is transferred from the modulated beam to the cavity to make up for losses in the cavity and load. It is apparent that oscillations are possible for transit times corresponding to $n + \frac{3}{4}$ cycles, where n is an integer.

With this much of an understanding of the qualitative behavior of the device, we proceed to take a more quantitative look.

For simplicity, the effect of space-charge forces on the electron motion will again be neglected. Because of the relatively low beam current of the reflex klystron, this is a good approximation everywhere except near the repeller where the electrons are reversing their direction of motion.

The tube has dc voltages applied as in Figure 9.2-1, with l being the spacing from gap to repeller. The polarities of gap voltage and induced current are taken as in Figure 9.1-5. Assume that there exists an rf voltage across the gap given by

$$v(t) = A \sin \omega t \tag{9.2-1}$$

The exit velocity of an electron is given by Equation (9.1-11),

$$u(d) = u_o\left(1 + \frac{M}{2}\frac{A}{V_o}\sin \omega t_o\right) \tag{9.2-2}$$

where t_o is the time at which the electron passes through the center of the gap.

We shall assume that there is a uniform electric field between the repeller and the cavity so that the electrons experience a uniform force directed toward the cavity while traveling in this region. The resulting acceleration of the electrons is given by the differential equation:

$$\frac{d^2z}{dt^2} = -\frac{e}{m}\frac{V_o + V_{Ro}}{l} \tag{9.2-3}$$

This equation can be integrated once, obtaining

$$\frac{dz}{dt} = u(d) - \frac{e}{m}\frac{V_o + V_{Ro}}{l}(t - t_o) \tag{9.2-4}$$

where t_o is the time at which the electron first passed the mid-point of the cavity. Strictly speaking, the exit time from the gap rather than t_o should be used in Equation (9.2-4).

Let us now find an expression for the time t at which the electron returns to the gap. This value is obtained by solving Equation (9.2-4), with

$$\frac{dz}{dt} = -u(d) \tag{9.2-5}$$

since the electron neither gains nor loses net energy in the repeller region. We obtain

$$t - t_o = \frac{2mlu_o}{e(V_o + V_{Ro})}\left[1 + \frac{M}{2}\frac{A}{V_o}\sin \omega t_o\right] \tag{9.2-6}$$

where use has been made of Equation (9.2-2). Multiplying through by the radian frequency, we obtain

$$\omega t - \omega t_o = \theta\left[1 + \frac{M}{2}\frac{A}{V_o}\sin \omega t_o\right] \tag{9.2-7}$$

where

$$\theta = \frac{2m\omega lu_o}{e(V_o + V_{Ro})} \tag{9.2-8}$$

is the dc transit angle in the repeller region.

To find an expression for the instantaneous current on the beam as it reenters the cavity, we proceed in the same manner as in Section 9.1, except that there is a different relationship between the departure and arrival times of an electron, that is, Equation (9.1-14) is replaced by (9.2-7). Comparing these two equations, we note that they are identical except for the algebraic sign of the term containing the bunching parameter X, where

$$X = \frac{M}{2}\frac{A}{V_o}\theta \tag{9.2-9}$$

The result for the reflex klystron therefore is given by Equation (9.1-24), except that X must be replaced by $-X$. We thus have the following result for the beam current injected into the cavity gap from the repeller region:

$$i(t) = -I_o - 2I_o\sum_{n=1}^{\infty}(-1)^n J_n(nX)\cos n(\omega t - \theta) \tag{9.2-10}$$

where use has been made of the identity[3]

[3]Reference 9.1, p. 128.

$$J_n(-x) = (-1)^n J_n(x) \tag{9.2-11}$$

The fundamental component of beam current is

$$i_1(t) = 2I_o J_1(X) \cos(\omega t - \theta) \tag{9.2-12}$$

In the notation of Figure 9.1-5, the electrons travel from right to left through the grids, so that the induced current phasor is given by

$$I = -2MI_o J_1(X)\epsilon^{-j\theta} \tag{9.2-13}$$

which is $-M$ times the phasor representing the current of Equation (9.2-12).

The equivalent circuit of the cavity is given as in the klystron amplifier by Figure 9.1-7, with one change. The beam-loading admittance is denoted by $g' + jb'$ instead of $g + jb$, since in a reflex klystron the results of Section 7.1(b) are not applicable. This is true for two reasons. First, the beam traverses the cavity twice and on its second transit is highly bunched. Second, the secondary electrons due to the beam impact contribute significantly to beam loading.

The induced current I acts as a current source producing the gap voltage V. This voltage in turn is the cause of the original velocity modulation on the electron stream.

When the tube is oscillating in the steady state, we may write

$$-\frac{I}{V} + G + jB = 0 \tag{9.2-14}$$

where

$$G = g' + G_c + G_L$$

and

$$B = b' + \omega C - \frac{1}{\omega L}$$

The amplitude and frequency of oscillation are determined by the condition that this equation be satisfied for both the real and imaginary parts. Let us define an electronic admittance by

$$Y_e = -\frac{I}{V} \tag{9.2-15}$$

Using Equations (9.2-1), (9.2-9) and (9.2-13), we have the following formula for the electronic admittance:

$$\begin{aligned} Y_e &= \frac{2MI_o J_1(X)\epsilon^{-j\theta}}{A\epsilon^{-j\frac{\pi}{2}}} \\ &= \frac{I_o M^2 \theta}{2V_o} \frac{2J_1(X)}{X} \epsilon^{j(\frac{\pi}{2}-\theta)} \end{aligned} \tag{9.2-16}$$

At oscillation, this admittance appears as a negative conductance shunted by some susceptance.

The electronic admittance is nonlinear since it is proportional to the factor

$$\frac{2J_1(X)}{X}$$

and X, the bunching parameter, is proportional to the rf gap voltage. This factor of proportionality is shown in Figure 9.2-3. As the magnitude of the

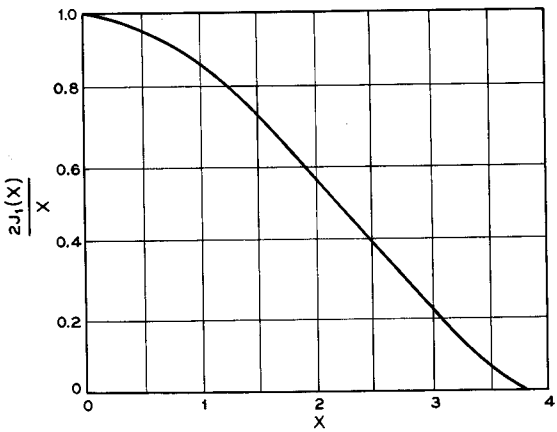

FIG. 9.2-3 Factor by which the electronic admittance varies with signal level. As the signal level goes to zero, this factor approaches unity.

rf gap voltage goes to zero, this factor approaches unity, and we obtain the small-signal value of the electronic admittance,

$$Y_{es} = \frac{I_o M^2 \theta}{2V_o} \epsilon^{j(\frac{\pi}{2}-\theta)} \tag{9.2-17}$$

When this admittance is plotted on a rectangular admittance chart as a function of θ, the dc transit angle, one obtains the admittance spiral shown in Figure 9.2-4. The admittance starts at the origin for zero transit angle and then spirals outward and clockwise as the transit angle is increased. Oscillations are possible for values of the transit angle which produce a negative conductance which is greater in magnitude than the positive conductance represented by the load and losses of the cavity. Maximum magnitudes of negative conductance are obtained for values of θ given approximately by $n + \frac{3}{4}$ cycles, where $n = 0,1,2$ etc. The electronic admittance spiral corresponding to any level of oscillation, that is, for a value of X

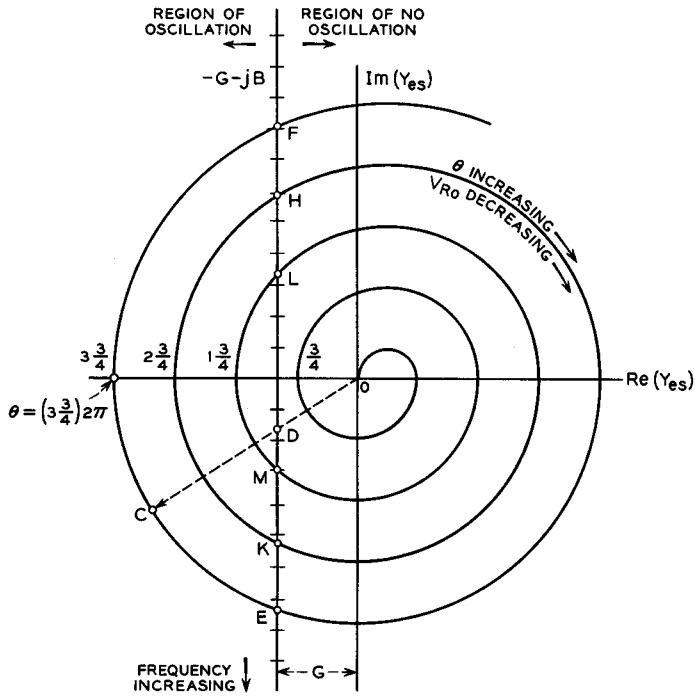

FIG. 9.2-4 Locus of small-signal electronic admittance Y_{es} on a rectangular impedance plot. The locus spirals out from the origin as the dc transit angle is increased from zero. Oscillations are obtained for negative conductances greater in magnitude than the total conductance loading the cavity, that is, for points to the left of the line $-G - jB$.

greater than zero, may be obtained from the small-signal spiral by shrinking the spiral radially by the factor $2J_1(X)/X$ obtained from Figure 9.2-3.

Equations (9.2-14) and (9.2-15) may be written as

$$Y_e = -(G + jB) \tag{9.2-18}$$

We now look for a graphical method of solving this equation so that oscillation power and frequency can be predicted as a function of the dc transit angle θ. For a fixed cavity geometry, the total shunt conductance G may be assumed constant over the frequency bandwidth of the cavity. The total shunt susceptance may be expanded as

$$\begin{aligned} B &= \omega C_T - 1/\omega L = C_T\left(\omega - \frac{\omega_o^2}{\omega}\right) \\ &= C_T\frac{(\omega + \omega_o)(\omega - \omega_o)}{\omega} \cong 2C_T\Delta\omega \cong 2GQ_l\frac{\Delta\omega}{\omega_o} \end{aligned} \tag{9.2-19}$$

where C_T is the gap capacitance plus a capacitance to account for beam loading, and Q_l is the loaded Q with the beam present, defined in Equation (9.1-32). ω_o is the radian resonant frequency with the beam present. We may plot

$$-(G + jB) = -G\left[1 + j2Q_l\frac{\Delta\omega}{\omega_o}\right] \tag{9.2-20}$$

as a function of frequency in Figure 9.2-4. The plot consists of a vertical line G units to the left of the origin. Equal increments of distance along the line correspond to equal increments of cycles off resonance. As the frequency is increased, the corresponding value of cavity admittance is found at a lower point on this line. By Equation (9.2-20) the frequency range between any two values of cavity admittance is inversely proportional to Q_l.

By Equation (9.2-18) an operating point in Figure 9.2-4 is found as the intersection of the cavity admittance locus EF and the electronic admittance spiral for the particular value of gap voltage. Thus in Figure 9.2-4 we note that small-signal oscillations ($X = 0$) are possible at the points E, F, H, K, L, and M, and the corresponding values of frequency and θ may be read off. From the values of θ, values of the repeller voltage are determined from Equation (9.2-8), given the beam voltage V_o.

How does one determine the operating conditions for higher levels of oscillation? Assume that the tube is oscillating at point E on the chart, and the repeller voltage is decreased so as to increase θ to correspond to the line OC. The small-signal admittance spiral has a larger magnitude of negative conductance than the positive value of cavity conductance. Hence oscillations will build up in amplitude and the admittance spiral will shrink until the conductances are equal in magnitude, that is, until point C recedes to point D on the shrunken spiral. An evaluation of the ratio of OD to OC gives the value of $2J_1(X)/X$, and hence the oscillation amplitude can be determined.

Oscillations of varying amplitude and frequency are produced continuously as one decreases the repeller voltage so as to move from point E along the line EF to point F. This whole range of operation is known as the $3\frac{3}{4}$ mode, since the center occurs at $\theta = 3\frac{3}{4}$ cycles. Similarly, the $2\frac{3}{4}$ mode of oscillation is produced over the range of transit angles needed to vary the electronic admittance from point K to point H. The $1\frac{3}{4}$ mode exists for transit angles needed to vary the electronic admittance from point M to point L. However, oscillations in the $\frac{3}{4}$ mode are not possible since the cavity conductance is too large; that is, the cavity is loaded too heavily to permit oscillation in this mode.

A physical description of the buildup of oscillations may also be presented with reference to Figure 9.2-4. Suppose the electron beam is suddenly

turned on with a set of electrode voltages corresponding to the line *ODC*. At this instant there exists an appreciable range of frequencies for which the net conductance is negative and also for which phase conditions are appropriate for positive feedback (note that this is *not* the frequency range corresponding to the line segment *ML*, since the latter range holds only for sinusoidal steady-state signals). Noise within this frequency range is amplified in a regenerative manner and builds up in amplitude. As the noise builds up, the negative conductance decreases in magnitude and the frequency range for regenerative amplification decreases. Finally, a stable operating condition is obtained for which the amplification bandwidth is sufficiently narrowed so that the product of the input noise power and the amplifier gain is equal to the output signal power. This bandwidth is so narrow that it corresponds practically to a single frequency. This description of oscillator operation is useful in analyzing such quantities as signal buildup-time and oscillation line width. It applies not only to the reflex klystron but also to all other types of sinusoidal oscillators.

By means of the graphical procedure described above one can plot curves

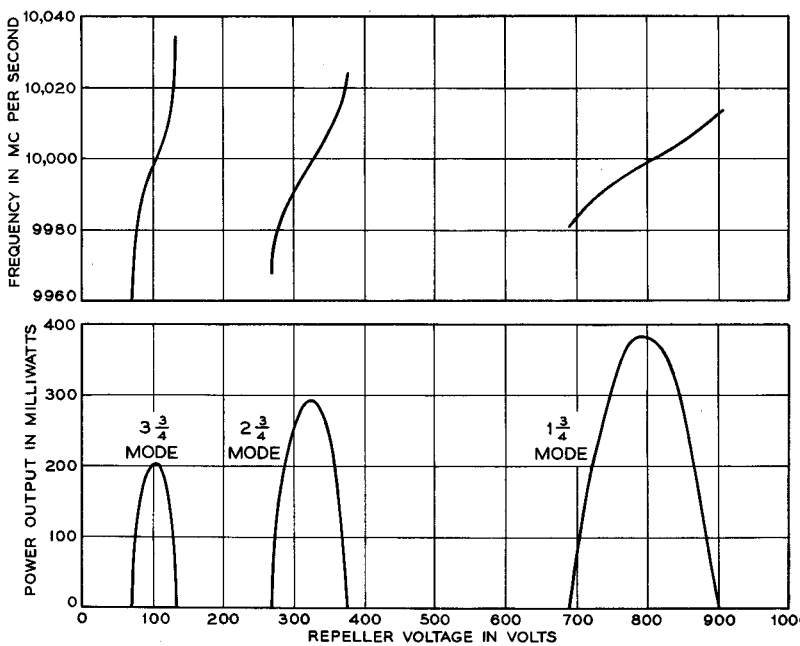

FIG. 9.2-5 Theoretical output characteristics of a reflex klystron. These curves were computed directly from Figures 9.2-3 and 9.2-4, with absolute values chosen so as to give results typical of commercially available tubes.

of power output and frequency vs. repeller voltage for any tube. Such curves are presented in Figure 9.2-5 where parameters have been chosen so as to obtain typical operating values. Three modes are obtained. For this example, modes of order higher than the $3\frac{3}{4}$ mode are not possible, since further reduction of the repeller voltage does not increase the transit time sufficiently to obtain the next higher mode. It should be noted that lower power output is obtained as the mode number is increased. From Equation (9.2-9) the gap voltage magnitude A is proportional to X/θ. Both X and θ increase with increasing mode number, but θ increases faster, so that the ratio X/θ decreases.

The reflex klystron has been the most common microwave tube for many years. With the cavity tuned to a nominal frequency, electronic tuning over a considerable bandwidth is possible merely by varying the repeller voltage. Since the repeller draws no beam current and since the capacitance from the repeller to ground may be made very small, the output frequency can be modulated by the simplest of electronic circuitry.

The reflex klystron is frequently used as a local oscillator in a microwave receiver; the electronic tuning obtainable is ideal for automatic frequency control. It is also commonly used as a laboratory signal source and as an FM transmitter frequency-deviator tube.

The plots of power output vs. repeller voltage presented in Figure 9.2-5 are typical. As the mode number is increased, wider tuning bandwidths are obtained, but the power output is decreased. Since wide tunability is usually the most desirable feature, most reflex klystrons are designed to operate in high-order modes, typically the $3\frac{3}{4}$, $4\frac{3}{4}$, and $5\frac{3}{4}$ modes. In order to obtain large bandwidth, Q_l is made quite low. However, the large value of G does not permit oscillations in the lower modes.

Different center frequencies may be obtained by tuning the cavity to different resonant frequencies and adjusting the repeller voltage. Cavity tuning is often accomplished by mechanical deformation of the cavity size using a bellows type of construction. The output power can be controlled by changing the beam voltage and current. The beam current can be controlled independently of the beam voltage if a control grid is included in the electron gun. This permits amplitude modulation of the output power.

An example of a reflex klystron is the WE-449A, shown in cross section in Figure 9.2-6. This tube uses an external type of cavity in which the inductive portion is largely outside of the vacuum envelope of the tube. A ceramic window separates the internal and external portions of the cavity. This type of construction greatly simplifies the mechanical tuning adjustment since the tuning adjustment can be made outside of the vacuum. In the 449A, this adjustment is made by the use of a plunger in the external cavity. The tube envelope is constructed entirely of metal and ceramic.

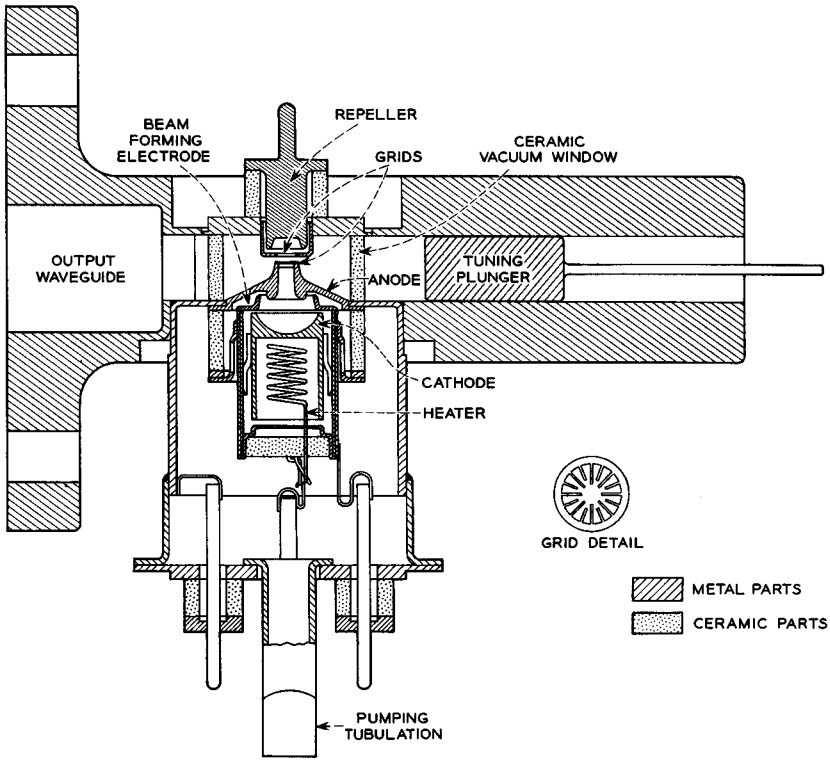

FIG. 9.2-6 WE-449A reflex klystron. This metal-ceramic tube has an overall height of approximately $6\frac{1}{2}$ cm and has the operating characteristics given in Table 9.2-1.

The electron gun is of the type shown in Figure 4.5-1(b), which generates a relatively high perveance beam of approximately 1 mm diameter. No magnetic field is used to prevent space-charge spreading of the beam, since the beam travels a relatively short distance.

The copper grids of the cavity have a geometry resembling the spokes of a

TABLE 9.2-1. WE-449A OPERATING CHARACTERISTICS

Frequency range, Mc	5925–6425
Beam voltage, volts	450
Beam current, ma	48
Perveance, amp/volt$^{3/2}$	5.03×10^{-6}
Repeller voltage, volts	75 to 125
Mode	$2\frac{3}{4}$
Power output, mw	125
Modulation sensitivity, Mc/volt	1.5

wheel in order to minimize electron interception. The gap spacing is 0.58 mm; the gap has a capacitance of 0.3 pf. The repeller electrode is cup-shaped in order to refocus the spreading beam so that it will pass through the grids on its return. The cavity has a hot unloaded Q_u of 135 and a hot loaded Q_l of 80.

The operating characteristics of the 449A are given in Table 9.2-1. The modulation sensitivity is defined as the ratio: (change in frequency of the output produced by a change in repeller voltage)/(change in repeller voltage). Greater than 40 mw of power is obtained over an electronically tunable bandwidth of 65 Mc.

9.3 Space-Charge Waves

Up to this point we have neglected the forces of mutual repulsion of the electrons. This has been justified insofar as we have considered low-power devices in which the density of electrons in the beam is small. However, in the next section and in further chapters, we shall consider high-power amplifier tubes in which the forces between electrons play an important role in modifying the rf performance. Therefore, we must study the forces which are produced by the bunches of electrons existing in tubes such as the klystron amplifier and the way in which these forces tend to modify the bunching process.

In Section 3.4, we have considered the forces due to dc space charge in electron beams, that is, in beams of uniform charge density with no bunching. Also discussed were the means of compensating for these forces using uniform or periodic axial magnetic fields or periodic axial electric fields. In the present section we shall consider the complementary effects of the rf bunches of electrons as a perturbation on the electron motion. We shall assume that the beam is confined to a nearly uniform diameter by one of the methods described in Section 3.4. It will be convenient to assume that the various quantities associated with an electron beam consist of a dc part plus an rf perturbation due to the electron bunches. In general, we shall assume that the rf perturbation is small compared with its dc counterpart.

(a) *A Graphic Illustration of Space-Charge Waves*

At this point it may be helpful to consider a graphic illustration of rf space-charge forces in an electron beam. Consider Figure 9.3-1. We wish to study two successive bunches of electrons as they travel down a drift tube at constant dc velocity. There is a nearly infinite magnetic field in the direction of travel so as to prevent radial excursions of the electrons. For simplicity, we shall assume that all the electrons in one transverse plane move as a unit, constituting an inflexible *disc* of charge. This is a good ap-

proximation for a thin beam. Although the electrons are moving to the right with an average velocity given by the dc voltage, we shall confine our attention to the relative motion of the discs. Thus, we shall view the motion from a frame of reference moving at the average electron velocity.

In Figure 9.3-1(a) are shown the discs comprising the two bunches at one instant of time. Discs D and H are at the centers of a bunch and anti-bunch, respectively. Thus, they have a velocity equal to the average

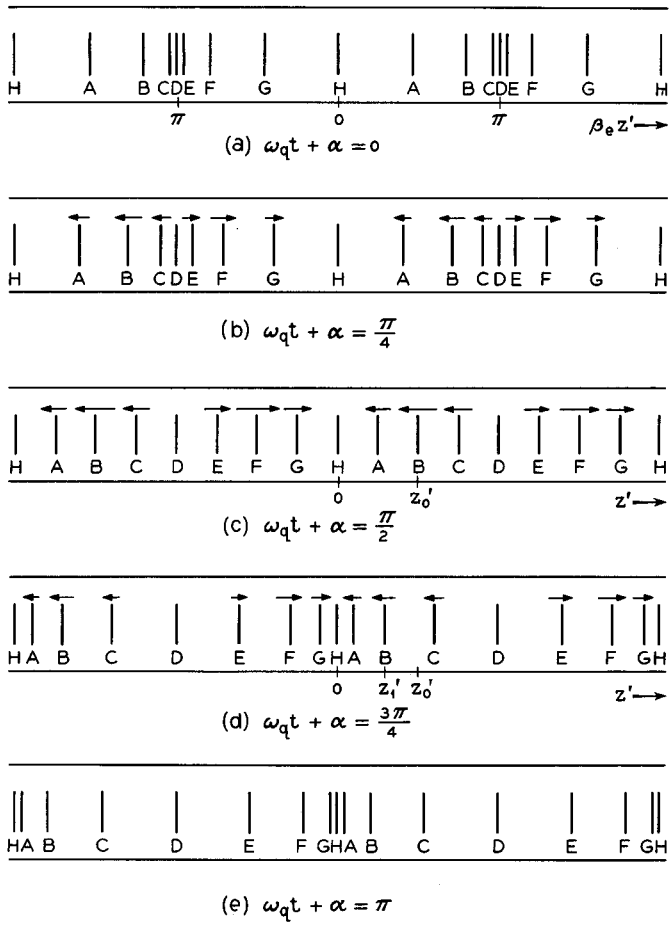

FIG. 9.3-1 Oscillations due to space-charge forces in a reference frame moving at the dc velocity of the electrons. Five successive instants of time are shown, separated by an eighth-cycle of the oscillation frequency. Instantaneous velocity vectors are shown above the charge discs.

velocity of the beam and remain stationary in our frame of reference. The center disc of the bunch exerts a repulsive force on the other discs in the bunch. Hence, discs A, B, and C are pushed to the left, whereas E, F, and G are pushed to the right.

Evidently the beam acts as an elastic medium, and oscillations of the discs in the axial direction will occur. A fraction of a cycle later in these oscillations the discs appear as in Figure 9.3-1(b). Discs A, B, and C are moving to the left (in the reference frame) and are still being accelerated in that direction by the space-charge force of the bunch. At the same time discs E, F, and G are moving and being accelerated to the right.

Still later, in Figure 9.3-1(c), the discs have attained a uniform spacing. However, they are not stationary in the reference frame. Discs A, B, and C are moving to the left, and discs E, F, and G to the right. Each disc sees as much space charge to the left as to the right; hence, the instantaneous acceleration is zero, and the discs have all reached their maximum velocity in the reference system. This is the instant for which the perturbation of charge density is zero; thus the rf components of velocity and charge density are 90 degrees out of phase.

An eighth of a cycle later, we have the situation depicted in Figure 9.3-1(d). A bunch is now beginning to form centered about disc H. The repulsive forces emanating from the center of this bunch act in such a direction as to slow down the motion to the left of discs A, B, and C. Similarly, the motion to the right of discs E, F, and G is also slowed down.

These electrons are finally brought to rest in the reference frame at the instant depicted in Figure 9.3-1(e). At this instant the instantaneous rf velocity is zero. The repulsive bunch is pushing to the right on discs A, B, and C, and to the left on discs E, F, and G.

For the next half cycle, the discs retrace their motions in the opposite directions, appearing as in Figure 9.3-1(d), (c), (b), and (a), successively. After arriving back at the positions in Figure 9.3-1(a), the cycle repeats itself. Thus the discs oscillate back and forth in the reference frame in a simple harmonic motion about the average positions shown in Figure 9.3-1(c).

(*b*) *Expressions for the AC Velocity, Charge Density, and Current Density*

From the preceding discussion, we can write equations describing the motion of the charge discs of Figure 9.3-1. Let us assume that the bunches are produced by an rf source of radian frequency ω at some distance to the left by some means such as a cavity gap. Since the beam velocity is u_o, the bunch spacing is given by

$$u_o \frac{2\pi}{\omega} = \frac{2\pi}{\beta_e} \tag{9.3-1}$$

where $\beta_e = \omega/u_o$.

Let z' be the axial coordinate in our frame of reference which moves with the dc beam velocity. We shall assume that the origin is at the location of electron disc H (which we have assumed stationary in this reference frame). Let ω_q be the frequency at which the discs oscillate back and forth in the reference frame.

If we assume that the velocity and charge-density perturbations are simple sinusoidal variations in both time and position, the behavior shown in Figure 9.3-1 may be described mathematically by the two equations:

$$\rho = B \cos \beta_e z' \cos(\omega_q t + \alpha) \tag{9.3-2}$$

$$u = -C \sin \beta_e z' \sin(\omega_q t + \alpha) \tag{9.3-3}$$

where ρ and u are the instantaneous rf charge density and velocity perturbations. B and C are positive constants determined by the magnitude of the rf perturbation, and α is a constant which determines the phase of the oscillations. The reader may verify that these relations hold for each of the instants illustrated in Figure 9.3-1. These two perturbations are seen to be 90 degrees out of phase in both time and axial position.

Equations (9.3-2) and (9.3-3) may be written in terms of the laboratory reference frame, where z is the axial position, using the relationship

$$z = z' + u_o t \tag{9.3-4}$$

obtaining

$$\rho = B \cos(\beta_e z - \omega t) \cos(\omega_q t + \alpha) \tag{9.3-5}$$

$$u = -C \sin(\beta_e z - \omega t) \sin(\omega_q t + \alpha) \tag{9.3-6}$$

The total charge density and velocity are given by

$$\rho_{tot} = -\rho_o + \rho \tag{9.3-7}$$

$$u_{tot} = u_o + u \tag{9.3-8}$$

where ρ_o is the magnitude of the electron charge density. Similarly, the total current density is written as

$$J_{tot} = -J_o + J \tag{9.3-9}$$

where J_o is the magnitude of the dc current density, and J is the rf perturbation. We shall refer to this current density in free space as convection current density in order to distinguish it from conduction current density flowing in a conductor. The positive direction for this current density is taken in the $+z$ direction.

The instantaneous convection current density at any point is defined as the product of the instantaneous velocity and charge density at that point. Thus, we have

$$J_{tot} = \rho_{tot} u_{tot} \tag{9.3-10}$$

or

$$-J_o + J = -\rho_o u_o + u_o\rho - \rho_o u + \rho u \tag{9.3-11}$$

We assume that the rf perturbation is small compared with the corresponding dc quantity; hence, the term ρu can be neglected in comparison with the other terms since it is the product of two small perturbations. Using the fact that $J_o = \rho_o u_o$, we obtain

$$J = u_o\rho - \rho_o u \tag{9.3-12}$$

The equation of continuity, Equation (1.3-2), can be written for the rf perturbations as

$$\frac{\partial J}{\partial z} = -\frac{\partial \rho}{\partial t} \tag{9.3-13}$$

since J is not a function of the transverse coordinates. From Equations (9.3-5), (9.3-6), and (9.3-12), we obtain

$$\frac{\partial J}{\partial z} = -\omega B \sin(\beta_e z - \omega t) \cos(\omega_q t + \alpha) + \beta_e \rho_o C \cos(\beta_e z - \omega t) \sin(\omega_q t + \alpha) \tag{9.3-14}$$

and

$$-\frac{\partial \rho}{\partial t} = -\omega B \sin(\beta_e z - \omega t) \cos(\omega_q t + \alpha) + \omega_q B \cos(\beta_e z - \omega t) \sin(\omega_q t + \alpha) \tag{9.3-15}$$

Equating these last two equations, we obtain

$$\omega_q B = \beta_e \rho_o C \tag{9.3-16}$$

relating the magnitudes of the velocity and charge-density rf variations. Using this relation, Equation (9.3-12) yields

$$J = u_o B \cos(\beta_e z - \omega t) \cos(\omega_q t - \alpha) + \frac{\omega_q}{\omega} u_o B \sin(\beta_e z - \omega t) \sin(\omega_q t + \alpha) \tag{9.3-17}$$

In practical microwave tubes ω_q/ω is small compared with unity, as we shall see later when we evaluate ω_q. Hence, the second term in this equation may be neglected in comparison with the first, and we obtain

$$J = u_o B \cos(\beta_e z - \omega t) \cos(\omega_q t + \alpha) \tag{9.3-18}$$

(c) *The Plasma Frequency*

Next, we shall obtain a method for determining ω_q, the frequency at which the space-charge forces cause the electrons to oscillate back and forth in the reference frame. In addition, we shall verify the sinusoidal behavior

assumed for the rf variations. We shall accomplish this by examining the electron motion of Figure 9.3-1 in a more quantitative fashion.

Our results will be derived for a one-dimensional beam, that is, for a beam that is uniform in the transverse direction and infinite in diameter. The oscillation frequency for this particular case will be designated ω_p. Later we shall show how the results can be altered to apply to a beam of finite cross-sectional area, with or without surrounding metal walls.

Starting with the case of a beam of infinite diameter, we note that if the discs in Figure 9.3-1 are uniformly spaced, as in Figure 9.3-1(c), there is no accumulation of charge at any position and hence no net electric field at any point. A uniform charge density $-\rho_o$ exists everywhere. Consider a typical disc, disc B, and let z_o' be its equilibrium position shown in Figure 9.3-1(c). In Figure 9.3-1(d), disc B has moved to a new position z_1'. This movement produces a charge excess in the region $0 \leq z' \leq z_1'$ over that which existed when the discs were uniformly spaced given by

$$\Delta q = -\rho_o(z_o' - z_1') \tag{9.3-19}$$

per unit area of the beam. This excess charge produces a restoring electric field at $z' = z_1'$ given by[4]

$$E_z = -\frac{\rho_o}{\varepsilon_o}(z_o' - z_1') \tag{9.3-20}$$

Thus, the acceleration of the electrons comprising a disc at any position z' is given by

$$\ddot{z}' = \frac{e}{m}\frac{\rho_o}{\varepsilon_o}(z_o' - z') \tag{9.3-21}$$

using Equation (1.1-1). This equation has the solution

$$z' - z_o' = F\cos(\omega_p t + \tau) \tag{9.3-22}$$

where

$$\omega_p^2 = \frac{e\rho_o}{m\varepsilon_o} \tag{9.3-23}$$

The frequency corresponding to ω_p is called the plasma frequency. It is proportional to the square root of the electronic charge density. This frequency

[4]The rf electric field as used here and in the remainder of this section is an rf perturbation on the dc electric field. As such, it represents a departure from the equilibrium value. Thus, it need not originate on positive charge and terminate on negative charge; rather, it originates on a *deficiency* of negative charge and terminates on an *excess* of negative charge. Some authors present a clearer physical picture by assuming the electron beam to be completely neutralized by immobile positive ions, so that rf electric field lines may originate on positive charges. This approach is not used here because it implies incorrectly that space-charge neutralization by positive ions is necessary for these space-charge waves to exist.

applies only to a beam of infinite diameter. Practical beams of finite diameter are characterized by a plasma frequency which is less than ω_p. This lower plasma frequency is called the reduced plasma frequency and is designated ω_q. F and τ are independent of time, but they may be functions of z_o', the relative position in the bunch. For example, for $\beta_e z_o'$ equal to 0 or π, F must be zero, since discs H and D are stationary in the reference frame.

The motion described by Equation (9.3-22) is simple harmonic motion of electrons about their equilibrium positions in the reference frame. Let us apply this result to the electrons leaving the input gap of a klystron amplifier. These electrons have a velocity given by Equation (9.1-11) at the exit of the gap,

$$u(d) = u_o + \frac{eMA}{mu_o} \sin \omega t_o \tag{9.3-24}$$

where t_o is the time at which the electrons pass through the gap. Since the electrons under the influence of the space-charge forces exhibit simple harmonic motion, the velocity at a later time t is given by

$$u_{\text{tot}} = u_o + \frac{eMA}{mu_o} \sin \omega t_o \cos \omega_p (t - t_o) \tag{9.3-25}$$

where ω_p corresponds to the frequency of the harmonic motion as discussed above.

The position of an electron disc is given by the product of the elapsed time and the average velocity to that instant. Since the rf perturbation of velocity is assumed small compared with the dc velocity, the average velocity is given approximately by u_o. Hence,

$$z = u_o(t - t_o) \tag{9.3-26}$$

This expression may be used to eliminate ωt_o from the sine term in Equation (9.3-25). Thus, we obtain

$$u_{\text{tot}} = u_o - \frac{eMA}{mu_o} \sin(\beta_e z - \omega t) \cos(\omega_p t - \omega_p t_o) \tag{9.3-27}$$

This result is identical to that given by Equation (9.3-6), deduced from Figure 9.3-1, if we take $\alpha = (\pi/2) - \omega_p t_o$ and $\omega_q = \omega_p$. Thus, in an infinite beam the electrons oscillate back and forth in the reference frame at the plasma frequency. In a beam of finite diameter, the restoring forces are somewhat weaker, and we shall find that the frequency of oscillation ω_q is less than ω_p.

The phase angle $\alpha = (\pi/2) - \omega_p t_o$ is essentially constant for any one bunch. This can be shown as follows. Over one cycle of the modulation on the beam, and hence over one bunch, t_o changes by $2\pi/\omega$, and $\omega_p t_o$ changes by $2\pi\omega_p/\omega$. Since at microwave frequencies ω_p/ω is usually small compared

with unity, the total variation in $\omega_p t_o$ over a bunch is small. In Figure 9.3-1 we have presented the results as though α were constant, for simplicity.

(*d*) *Beams of Finite Diameter*

The results we have derived so far have been derived for an electron beam infinite in cross-sectional area. All practical beams are, of course, of finite diameter; hence, we should inquire how the foregoing results are modified for a finite beam.

Let us return to a consideration of the forces between discs of charge. It will be easier for us to visualize the rf electric field lines if we can have them begin on positive charges and end on negative charges.[5] Since these field lines are due to excess charge (from the equilibrium value) in any region, we can picture a deficiency of negative charge in any region as a positive charge. The electric field lines due to the equilibrium charge density $-\rho_o$ are not considered at all, since the beam is assumed to be confined by one of the focusing schemes of Section 3.4. In other words, the electric field we shall depict is the difference between the total instantaneous electric field and the dc electric field at any point.

The situation for an infinite beam is shown in Figure 9.3-2(a). The negative discs of charge (shown shaded) are clustered around the center of the electron bunch. The positive discs (unshaded) are clustered around the antibunch. The electric field lines in this case are given by straight horizontal lines from the positive to the negative discs.

In Figure 9.3-2(b) the analogous situation is shown for a beam of finite diameter. The electric field lines are no longer straight horizontal lines, but instead they bow out. Thus, the axial component of electric field at any disc is reduced in magnitude. This occurs for two reasons. First, the bowing out of the field lines increases the area through which the total electric flux passes. Second, the tilting of the field lines means that only a portion of the total field exists as an axial component.

As a consequence of the weakening of the axial electric field, the total restoring force on a disc is reduced. Hence, Equation (9.3-20) may be written as

$$E_z = -R^2 \frac{\rho_o}{\varepsilon_o}(z_o' - z_1') \tag{9.3-28}$$

where R^2 is a number less than unity and is a function of the beam diameter. The differential equation of motion (9.3-21) is altered by the same factor, and one thus obtains the solution:

$$z' - z_o' = F \cos(R\omega_p t + \theta) \tag{9.3-29}$$

---

[5]See footnote 4.

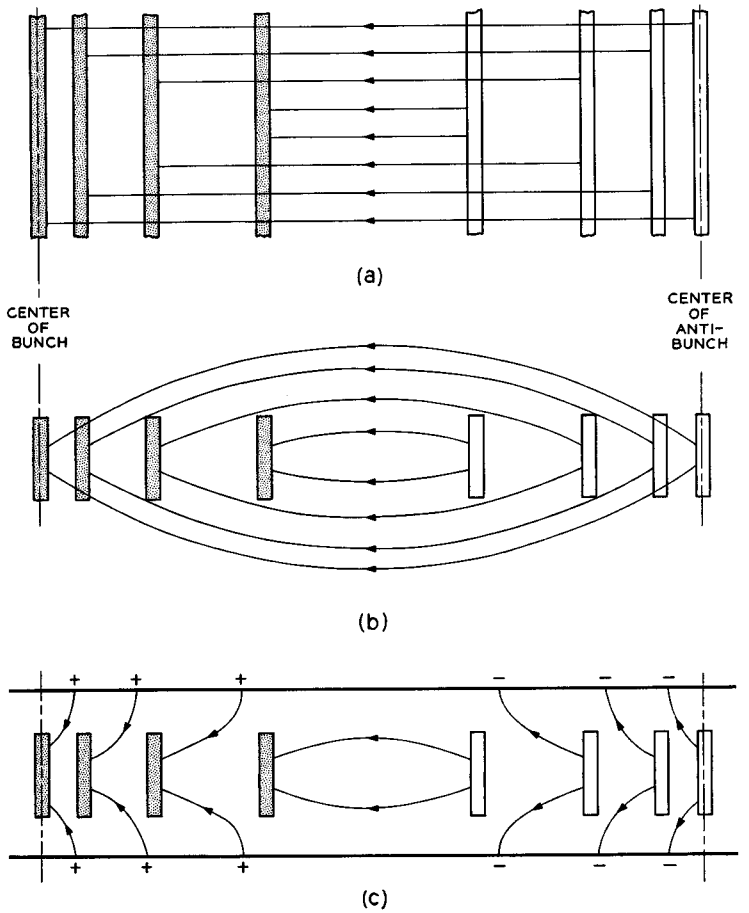

FIG. 9.3-2 RF electric field lines in various beams. Positively charged discs (unshaded discs) are used in regions where the instantaneous electron density is below the dc value. The shaded discs are negatively charged and represent electron densities above the dc value. (a) Portion of an infinite beam in which all quantities are uniform in the transverse directions. The rf electric field lines are straight and parallel to the direction of electric flow. (b) Beam of finite diameter. (c) Finite diameter beam in a drift tube.

for the finite beam, instead of Equation (9.3-22). R is known as the space-charge reduction factor, and we may define the reduced plasma frequency as

$$\omega_q = R\omega_p \tag{9.3-30}$$

All of the results derived for the infinite beam are directly applicable to the finite beam. It is necessary only to replace ω_p by ω_q. Implicit in this development is the requirement of a strong axial magnetic field so that radial excursions of the electrons due to transverse rf electric fields are prevented.

In Figure 9.3-2(c) is shown the field pattern obtained when the beam is surrounded by a metal cylinder. Many of the field lines terminate on charges on the metal wall. This further reduces the restoring force which tends to bring the discs back to their equilibrium positions. Thus, the reduction factor R is seen to be a function of both the beam diameter and the proximity of a metal wall. As the wall comes closer to the beam, the space-charge forces become smaller, and the frequency of oscillation depicted in Figure 9.3-1 becomes smaller.

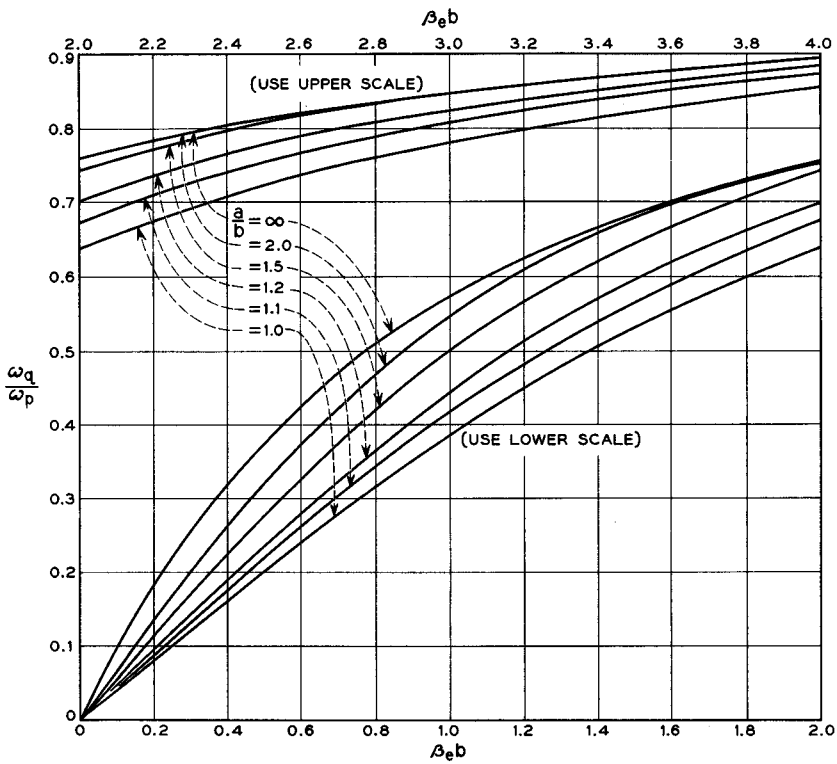

FIG. 9.3-3 Plasma frequency reduction factor vs. beam diameter for a solid, cylindrical beam of radius b in a concentric, perfectly conducting cylinder of radius a (Reference 9.3). (Courtesy of *Transactions IRE*)

Values of the space-charge reduction factor have been calculated for various kinds of beams with surrounding metal walls.[6] These results have been obtained by solving Maxwell's Equations inside and outside of an idealized electron beam, such as we have considered, and matching boundary conditions at the surface of the beam. Figure 9.3-3 shows the result for a solid cylindrical beam centered in a perfectly conducting metal cylinder. The reduction factor is plotted as a function of $\beta_e b = \omega b/u_o$, where b is the beam radius. a is the radius of the conducting cylinder. Several curves are given, each for a different ratio of cylinder diameter to beam diameter. Most microwave tubes have beams with $\beta_e b$ in the range 0.5 to 1.0, so that the reduction factor is typically $\frac{1}{3}$ to $\frac{1}{2}$.

Let us determine the ratio ω_q/ω for a microwave tube with the following properties:

Beam voltage, volts	2400
Beam current, ma	40
Beam diameter, mm	1.3
Wall diameter, mm	2.3
Frequency, Mc	6000

We shall describe a traveling-wave tube with these parameters in Chapter 10. From these data we obtain:

$$\rho_o = 1.04 \times 10^{-3} \text{ coulomb/meter}^3$$

$$\frac{\omega_p}{\omega} = 0.12$$

$$\beta_e b = 0.84$$

From Figure 9.3-3 we find that

$$R = 0.46$$

so that

$$\frac{\omega_q}{\omega} = 0.055$$

This confirms the previous assumptions that ω_q/ω is small compared with unity in a typical case.

The rf part of Equation (9.3-27) for the instantaneous velocity can be written in a more convenient form as

$$u = -\frac{1}{2} u_o M \frac{A}{V_o} \cos \beta_q z \sin(\beta_e z - \omega t) \tag{9.3-31}$$

[6]Reference 9.3.

where we have substituted for $t - t_o$ from Equation (9.3-26), and we have set

$$\beta_q = \frac{\omega_q}{u_o} \tag{9.3-32}$$

We use ω_q here instead of ω_p so that the results will be applicable to beams of finite diameter. Since β_q is much less than β_e, Equation (9.3-31) represents a wave propagating with a phase velocity equal to the dc beam velocity and whose amplitude is slowly changing with distance. A plot of this equation vs. distance at the instant $\omega t = \pi/2$ is shown in the upper half of Figure 9.3-4.

The equation for the current density may be obtained from Equation (9.3-18) in the same manner. Thus

$$J = -\frac{1}{2} J_o \frac{\omega}{\omega_q} M \frac{A}{V_o} \sin \beta_q z \cos(\beta_e z - \omega t) \tag{9.3-33}$$

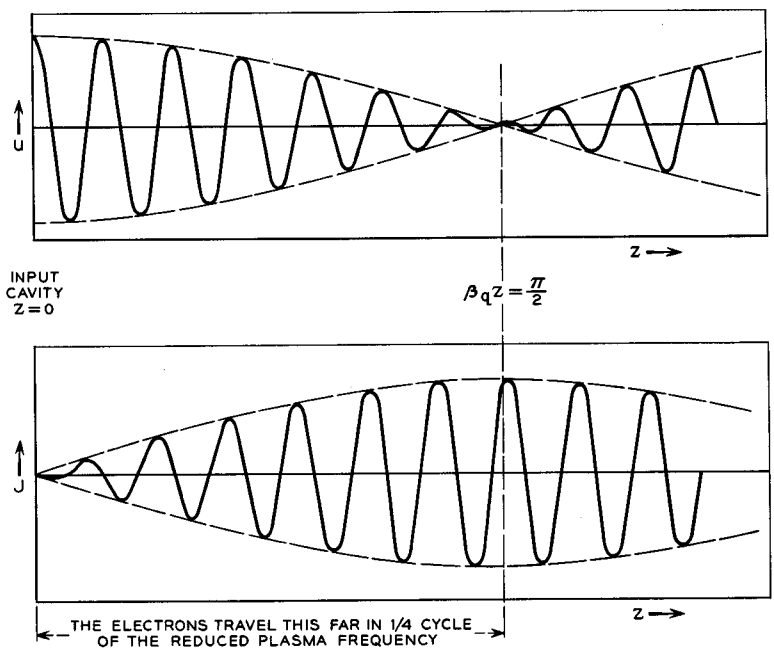

FIG. 9.3-4 Variation with distance of the rf velocity and convection current density for an electron beam which receives velocity modulation from an input cavity placed at $z = 0$. The output cavity is placed at $\beta_q z = \pi/2$ to obtain maximum induced current. The waveforms are shown at a particular instant of time. The envelopes remain stationary, whereas the sinusoidal waves within move to the right at the dc velocity.

where use has been made of Equations (9.3-6), (9.3-16), (9.3-18), (9.3-31) and the fact that $\alpha = \pi/2 - \omega_q t_o$, and $J_o = u_o \rho_o$. J is plotted in the lower half of Figure 9.3-4 for the instant $\omega t = \pi/2$.

From Figure 9.3-4 we note that the velocity modulation magnitude is a maximum at the position of the input cavity gap. Beyond the gap, the velocity modulation magnitude varies as $|\cos \beta_q z|$, whereas the current modulation magnitude varies as $|\sin \beta_q z|$. At a position given by

$$\beta_q z_{\text{opt}} = \frac{\pi}{2} \tag{9.3-34}$$

the current modulation has become a maximum and the velocity modulation is zero. This distance may be termed a quarter-plasma wavelength. If one were to construct a two-cavity klystron, the output cavity would be placed at this distance from the input cavity in order to obtain maximum induced current in the output cavity.

At this point it will be well to note that the foregoing solutions are small-signal solutions, albeit space-charge forces are included. By comparison, the solutions of Section 9.1(b) are applicable under larger signal conditions — limited chiefly by the approximation in going from Equation (9.1-12) to (9.1-13) — but neglecting space-charge forces. The more general problem of large signal interaction with space charge considered requires elaborate computer calculations for solution.[7]

Thus we have from Equation (9.3-33) the result that with space charge at small signal levels the maximum current modulation occurs at the position given by Equation (9.3-34) with a magnitude

$$\frac{i_1}{I_o} = \frac{1}{2} \frac{\omega M A}{\omega_q V_o} \tag{9.3-35}$$

This may be compared with the results of Section 9.1(b) for a finite signal level, but neglecting space charge. From Equation (9.1-24) we have the result that the maximum current modulation is given by

$$\frac{i_1}{I_o} = 1.16 \tag{9.3-36}$$

at a position corresponding to

$$\beta_q z_{\text{opt}} = 3.68 \frac{\omega_c V_o}{\omega M A} \tag{9.3-37}$$

These limiting results may be compared with the numerical results obtained by Webber which include both space charge and finite signal level.[8] Figure

[7]Reference 9.4.
[8]Reference 9.4.

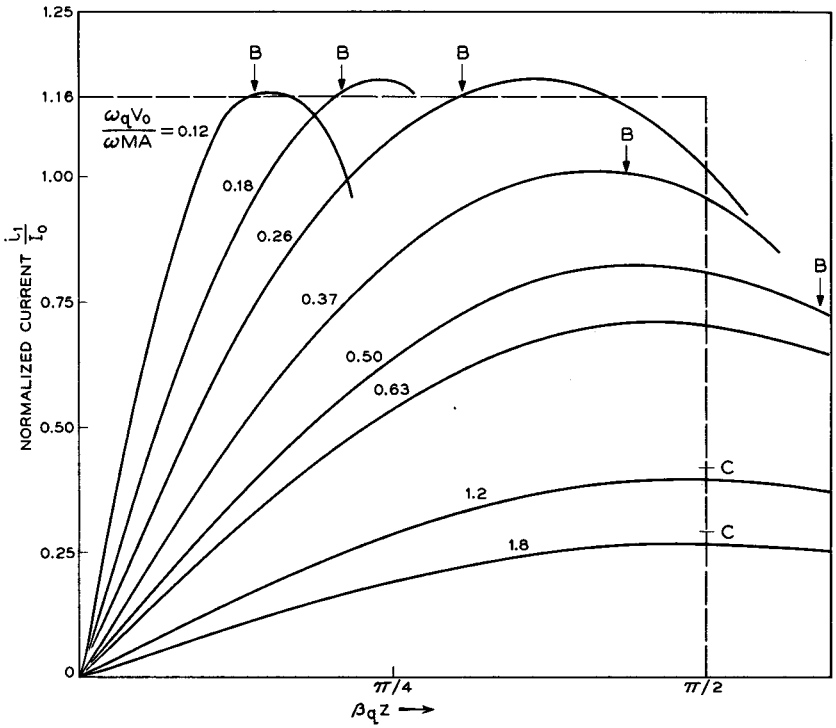

FIG. 9.3-5 Variation of the magnitude of the fundamental component of convection current with distance from the input gap, as given by computer calculations. For a beam of fixed voltage and current, the different curves represent operation at different input signal voltages, A. The nonlinear theory, neglecting space charge, developed in Section 9.1 predicts a nonvarying maximum value of 1.16 occurring at values of the abscissa marked B for five of the curves. The small-signal, space-charge theory developed in this section predicts maxima as given by levels marked C for two of the curves, occurring at a fixed distance given by one quarter of a reduced plasma wavelength. The limits of applicability of the two theories are readily apparent (Reference 9.4). (Courtesy of *Transactions IRE*)

9.3-5 shows Webber's calculated plots of the magnitude of the fundamental component of current modulation vs. distance from the input cavity for various values of the parameter $\omega_q V_o/\omega MA$, which we have seen appears in Equations (9.3-35) and (9.3-37). This parameter may be considered to show the variation with input-cavity-signal level A for a given electron beam, wherein ω_q, ω, V_o, and M are constant. At small signal levels, Equations (9.3-34) and (9.3-35) are seen to hold, whereas, as the signal level is increased, the values given by Equations (9.3-36) and (9.3-37) are obtained.

(e) *Fast and Slow Space-Charge Waves*

The variation of the magnitude of the velocity and current density with distance as shown in Figure 9.3-4 has the appearance of a standing wave. Alternatively the behavior may be written as the sum of two traveling-wave disturbances. Thus, Equations (9.3-31) and (9.3-33) may be written, respectively, as

$$u = \frac{1}{4}u_o M \frac{A}{V_o}[\sin(\omega t - \beta_f z) + \sin(\omega t - \beta_s z)] \tag{9.3-38}$$

and

$$J = -\frac{1}{4}J_o \frac{\omega}{\omega_q} M \frac{A}{V_o}[\sin(\omega t - \beta_f z) - \sin(\omega t - \beta_s z)] \tag{9.3-39}$$

where

$$\beta_f = \beta_e - \beta_q \tag{9.3-40}$$

and

$$\beta_s = \beta_e + \beta_q \tag{9.3-41}$$

These two traveling waves are known as the fast and slow space-charge waves, since their phase velocities are respectively faster and slower than the dc beam velocity.[9]

The fast and slow space-charge waves are two normal modes of excitation possible on a constant-dc-velocity electron beam in a drift tube. This means that each wave may exist by itself, or any combination of the two may exist. The input gap in a klystron excites the two waves such that the two velocity components are equal in magnitude and phase at the gap, whereas the current-density components are equal in magnitude but opposite in phase. The two different phase constants β_f and β_s acting over a distance given by Equation (9.3-34) bring the current density components into phase and the velocity components 180 degrees out of phase. Thus, when space-charge effects are taken into account, the klystron interaction principle may be thought of as an interference effect between the fast and slow space-charge waves.

As a final point, let us consider how the two-cavity klystron can be used to excite an electron beam with only the slow space-charge wave in the region beyond the output cavity. Let the input cavity produce the velocity and current-density variations given by Equations (9.3-31) and (9.3-33).

---

[9]Strictly speaking, the abscissa in Figure 9.3–3 should be $\beta_f b$ or $\beta_s b$ instead of $\beta_e b$ and the space-charge reduction factor R should be computed separately for each space-charge wave. However, since $\beta_q \ll \beta_e$, little error is introduced by using $\beta_e b$ for this computation.

The output cavity is placed a quarter-plasma-wavelength away, and the rf convection current induces current in the cavity. Let us adjust the loading of the output cavity so that this induced current produces an output gap voltage given by

$$-A\cos\left(\omega t - \frac{\pi}{2}\frac{\omega}{\omega_q}\right) = A\sin\left(\omega t - \frac{\pi}{2}\frac{\omega}{\omega_q} - \frac{\pi}{2}\right) \tag{9.3-42}$$

Note that this requires simply a conductance of proper value for the equivalent circuit of the output cavity and load. The velocity and current-density variations produced by this second gap voltage alone may be obtained from Equations (9.3-31) and (9.3-33) by replacing ωt by

$$\omega t - \frac{\pi}{2}\frac{\omega}{\omega_q} - \frac{\pi}{2}$$

and $\beta_q z$ by

$$\beta_q z - \frac{\pi}{2}$$

One obtains after simplification:

$$u_2 = -\frac{1}{2}u_o M\frac{A}{V_o}\sin\beta_q z\cos(\beta_e z - \omega t) \tag{9.3-43}$$

and

$$J_2 = -\frac{1}{2}J_o\frac{\omega}{\omega_q}M\frac{A}{V_o}\cos\beta_q z\sin(\beta_e z - \omega t) \tag{9.3-44}$$

In the region beyond the output cavity the modulation produced is the superposition of the variations produced by the two gap voltages. When Equations (9.3-31) and (9.3-43) are added and simplified, one obtains

$$u_s = -\frac{1}{2}u_o M\frac{A}{V_o}\sin(\beta_s z - \omega t) \tag{9.3-45}$$

Similarly, Equations (9.3-33) and (9.3-44) are added to give

$$J_s = -\frac{1}{2}J_o\frac{\omega}{\omega_q}M\frac{A}{V_o}\sin(\beta_s z - \omega t) \tag{9.3-46}$$

Comparing these results with Equations (9.3-38) and (9.3-39), we see that we have obtained purely a slow space-charge wave, whose amplitude is twice as large as that of either space-charge wave in the drift region between cavities.

9.4 Multicavity Klystron Amplifiers

Most klystron amplifiers are high-power tubes wherein the rf space-charge forces are quite important. Therefore, it is necessary to use the

space-charge wave theory developed in the previous section to evaluate properly the performance characteristics of these tubes. Let us first consider these relations as they apply to the two-cavity klystron amplifier of Figure 9-2.

The rf velocity and current-density variations between the input and output cavities are as shown in Figure 9.3-4. The output cavity is placed at the point where the rf current modulation is a maximum, that is, at $\beta_q z = \pi/2$. For simplicity, the two cavities are assumed to be identical. From Equation (9.3-33) the magnitude of the rf convection current at the output cavity is given by

$$|i_2| = \frac{1}{2} I_o \frac{\omega}{\omega_q} M \frac{A}{V_o} \tag{9.4-1}$$

From the discussion given in Section 9.1(c), the magnitude of the current induced into the output cavity is equal to[10]

$$|I_2| = M|i_2| = \frac{1}{2} I_o \frac{\omega}{\omega_q} M^2 \frac{A}{V_o} \tag{9.4-2}$$

The equivalent circuit of the output cavity is given in Figure 9.1-7, The magnitude of the impedance of a parallel circuit of this type can be written as[11]

$$|Z_2| = \frac{1}{G_T \sqrt{1 + 4Q_l^2 \left(\frac{\Delta f}{f_o}\right)^2}} \tag{9.4-3}$$

where

G_T is the total shunt conductance
Q_l is the hot loaded Q of the cavity
f_o is the resonant frequency
Δf is the departure of the operating frequency from f_o

For the output circuit,

$$G_T = G_c + g + G_L \tag{9.4-4}$$

where the symbols are defined in Figure 9.1-7. The output cavity is assumed matched to the load for maximum power transfer, that is,

$$G_L = G_c + g \tag{9.4-5}$$

---

[10]The results of section 9.1(c) are applicable under the assumption that $\omega_q \ll \omega$ and the output gap is short. Under these conditions, the convection current may be written as in Equation (9.1-25).

[11]Reference 9.5.

The power delivered to the load is therefore given by

$$P_{\text{out}} = \tfrac{1}{2} \mid I_2 \mid^2 \mid Z_2 \mid^2 G_L$$

$$= \frac{1}{32}\left(\frac{I_o}{V_o}\right)^2\left(\frac{\omega}{\omega_q}\right)^2 \frac{M^4 A^2}{G_{ch}} \frac{1}{1 + 4Q_l^2\left(\frac{\Delta f}{f_o}\right)^2} \tag{9.4-6}$$

where G_{ch} is defined in terms of the hot unloaded Q of the cavities;

$$G_{ch} \equiv G_c + g \tag{9.4-7}$$

The subscript *ch* is used here to designate "(unloaded) cavity hot." The input power is the power delivered to the input cavity by the source. From Figure 9.1-8, we obtain

$$P_{\text{in}} = \tfrac{1}{2} A^2 G_{ch} \tag{9.4-8}$$

The power gain is given by the ratio of P_{out} to P_{in}:

$$\underset{\text{(2-cav. klystron)}}{\text{power gain}} = \frac{M^4}{16}\left(\frac{\omega}{\omega_q}\right)^2\left(\frac{I_o}{V_o}\right)^2 \frac{1}{G_{ch}^2} \frac{1}{1 + 4Q_l^2\left(\frac{\Delta f}{f_o}\right)^2} \tag{9.4-9}$$

Let us examine the gain expression in detail. The last factor determines approximately the frequency dependence of the gain. The power is reduced to one half when $\Delta f/f_o = 1/2Q_l$, so that the half-power bandwidth is given by

$$\text{half-power bandwidth} = f_o/Q_l \tag{9.4-10}$$

Thus the bandwidth varies inversely with the loaded Q of the output cavity. However, by virtue of the term $1/G_{ch}^2$, the power gain is proportional to the square of the cavity Q's. Therefore it is possible to trade gain for bandwidth by adjusting the cavity Q's. Normally, two-cavity klystrons are designed for maximum cavity Q's, obtaining maximum gain and efficiency and accepting whatever bandwidth is produced. Thus, the klystron amplifier is inherently a narrow-band device.

From Equations (9.3-23) and (9.3-30) we have the following proportionality:

$$\omega_q^2 \propto \rho_o \propto \frac{I_o}{\sqrt{V_o}} \tag{9.4-11}$$

Consequently, the term $(\omega/\omega_q)^2 (I_o/V_o)^2$ in Equation (9.4-7) is proportional to $I_o/V_o^{3/2}$. This means that the power gain given by Equation (9.4-9) is proportional to the beam perveance, as defined in Section 4.5. Thus high perveance electron guns are needed in order to achieve high gain. Gains of 10 db or so are often obtained with two-cavity tubes.

One way of achieving higher overall gain is to connect several two-cavity amplifier tubes, in series, each tube providing approximately 10 db of gain. The power gain of two identical tubes in series is given by squaring the right-hand side of Equation (9.4-9),

$$\text{power gain (2 klystrons)} = \frac{M^8}{256}\left(\frac{\omega}{\omega_q}\right)^4\left(\frac{I_o}{V_o}\right)^4\frac{1}{G_{ch}{}^4}\frac{1}{\left[1+4Q_l{}^2\left(\frac{\Delta f}{f_o}\right)^2\right]^2} \tag{9.4-12}$$

where it is assumed that input and output ports are all matched to their transmission lines. A power gain of 40 db might be achieved by connecting four 10-db tubes in series.

High gain is achieved in a much simpler fashion using the multicavity klystron amplifier. A three-cavity klystron amplifier is illustrated in Figure 9.4-1. The construction of this tube is similar to the two-cavity amplifier, differing solely in the number of cavities. The tube functions in the following manner. The input signal impresses velocity modulation on the beam at the input cavity gap. The second cavity is placed a quarter of a plasma wavelength away at the position of maximum rf convection current modulation. The induced current in this cavity produces a voltage across its gap.

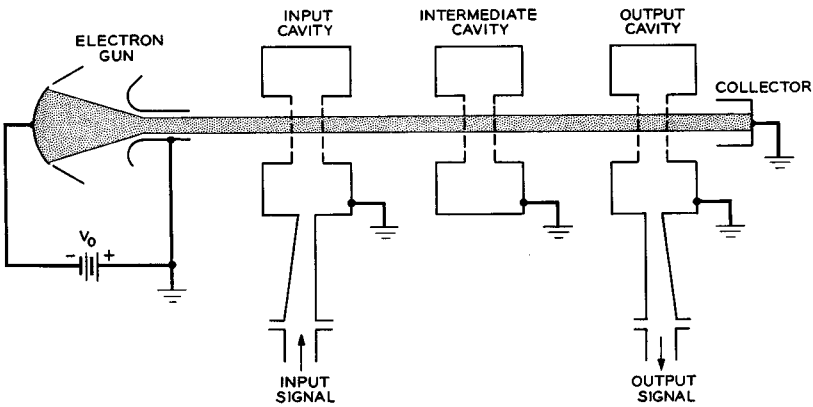

FIG. 9.4-1 Three-cavity klystron amplifier.

This second cavity voltage, which is considerably larger than the first cavity voltage, impresses velocity modulation on the beam at this point. This velocity modulation produces current modulation at the output cavity, a quarter-plasma-wavelength away. The rf convection current passing through the output cavity produces an induced current in the output cavity which causes rf power to be delivered to the load.

Thus we see that the three-cavity klystron amplifier is very much like two two-cavity tubes placed end-to-end. The basic difference is that the output cavity of the first tube and the input cavity of the second tube are combined into one intermediate cavity in the three-cavity tube.

Let us carry out a simplified analysis of the three-cavity amplifier, Assume that all three cavities are identical; that is, all have the same unloaded Q and beam-coupling coefficient. The intermediate cavity is not externally loaded, but the input and output cavities are matched to their transmission lines.

If A is the magnitude of the input-cavity-gap voltage, the magnitude of the rf convection current injected into the intermediate cavity gap is given by Equation (9.4-1), as for the output cavity in the two-cavity tube. The induced current in the intermediate cavity is given by Equation (9.4-2). The magnitude of the gap voltage produced by this current is given by

$$|V_2| = \frac{1}{2}\frac{\omega}{\omega_q}\frac{I_o}{V_o}\frac{M^2A}{G_{ch}}\frac{1}{\sqrt{1+4Q_u^2\left(\frac{\Delta f}{f_o}\right)^2}} \tag{9.4-13}$$

where Q_u is the hot unloaded Q of the cavity. This voltage produces a velocity modulation on the beam, which is converted into an rf convection current at the output cavity of a magnitude given by Equation (9.4-1), with A replaced by $|V_2|$, that is

$$|i_3| = \frac{1}{4}\left(\frac{\omega}{\omega_q}\right)^2\left(\frac{I_o}{V_o}\right)^2\frac{M^3A}{G_{ch}}\frac{1}{\sqrt{1+4Q_u^2\left(\frac{\Delta f}{f_o}\right)^2}} \tag{9.4-14}$$

The current induced in the output cavity is M times this value. The power delivered to a matched load is given by

$$P_{\text{out}} = \frac{M^2|i_3|^2}{8G_{ch}}\frac{1}{1+4Q_l^2\left(\frac{\Delta f}{f_o}\right)^2} \tag{9.4-15}$$

which, together with the expression for $|i_3|$, becomes

$$P_{\text{out}} = \frac{M^8}{128}\left(\frac{\omega}{\omega_q}\right)^4\left(\frac{I_o}{V_o}\right)^4\frac{A^2}{G_{ch}{}^3}\frac{1}{1+4Q_u^2\left(\frac{\Delta f}{f_o}\right)^2}\frac{1}{1+4Q_l^2\left(\frac{\Delta f}{f_o}\right)^2} \tag{9.4-16}$$

The input power is given by Equation (9.4-8), so that the gain is

$$\text{power gain (3-cav. klystron)} = \frac{M^8}{64}\left(\frac{\omega}{\omega_q}\right)^4\left(\frac{I_o}{V_o}\right)^4\frac{1}{G_{ch}{}^4}\frac{1}{1+4Q_u^2\left(\frac{\Delta f}{f_o}\right)^2}\frac{1}{1+4Q_l^2\left(\frac{\Delta f}{f_o}\right)^2} \tag{9.4-17}$$

Comparing this expression with Equation (9.4-12), which gives the gain of two two-cavity tubes in cascade, we note that the three-cavity tube has four times as much power gain at midband. However, we note that it also has less bandwidth by virtue of the fact that $Q_u = 2Q_l$. If we were to load the intermediate cavity by an external load so as to obtain Q_l instead of Q_u for this cavity, the two expressions for gain would be identical. For applications where bandwidth is not important, the higher gain made possible by using an unloaded intermediate cavity is a distinct advantage.

Still higher gain may be obtained by adding additional intermediate cavities. Multicavity klystrons with as many as seven cavities are commercially available, although the most frequently used number of cavities is four. Each of the intermediate cavities functions in the same manner as in the three-cavity amplifier. Gains of greater than 60 db are obtained when the cavities are synchronously tuned, that is, all tuned to the same frequency. However, often multicavity klystrons are operated with their cavities stagger-tuned so as to obtain greater bandwidth at some reduction in gain. This is analogous to the well-known design of wide-band IF amplifiers, wherein each stage is tuned to a slightly different frequency so as to improve the overall gain-bandwidth product. High-power klystron amplifiers with 40 to 50 db of gain and bandwidths equal to several per cent of the midband frequency are commercially available.

In high-power klystrons the cavity grids are omitted, since they would burn up due to beam interception. The beam-coupling coefficient in this case is given by a more complicated expression than Equation (9.1-10), but otherwise the interaction is unchanged.

Figure 9.4-2 shows two photographs of the Varian Associates VA-849,[12] which produces an output power of 24 kw CW (continuous wave). A cross-sectional drawing of the tube is shown in Figure 9.4-3. The tube can be purchased with cavities tuned to operate at any center frequency in the range 7125 to 8500 Mc. It is about 45 cm long and weighs 14 pounds. Figure 9.4-2(b) shows the tube in place in its electromagnet. The magnet weighs 200 pounds and dissipates a power of 1520 watts. It provides the axial dc magnetic field for focusing the beam.

The operating characteristics of the VA-849 are given in Table 9.4-1. The tube has four cavities, each with a cold unloaded Q_o of about 5000. Data are presented in the table for the synchronously tuned situation and also for the case when the third cavity has its resonant frequency tuned higher. The cavity gaps are equally spaced by a distance corresponding to approximately one ninth of a plasma wavelength. This spacing, rather

---

[12]Reference 9.6.

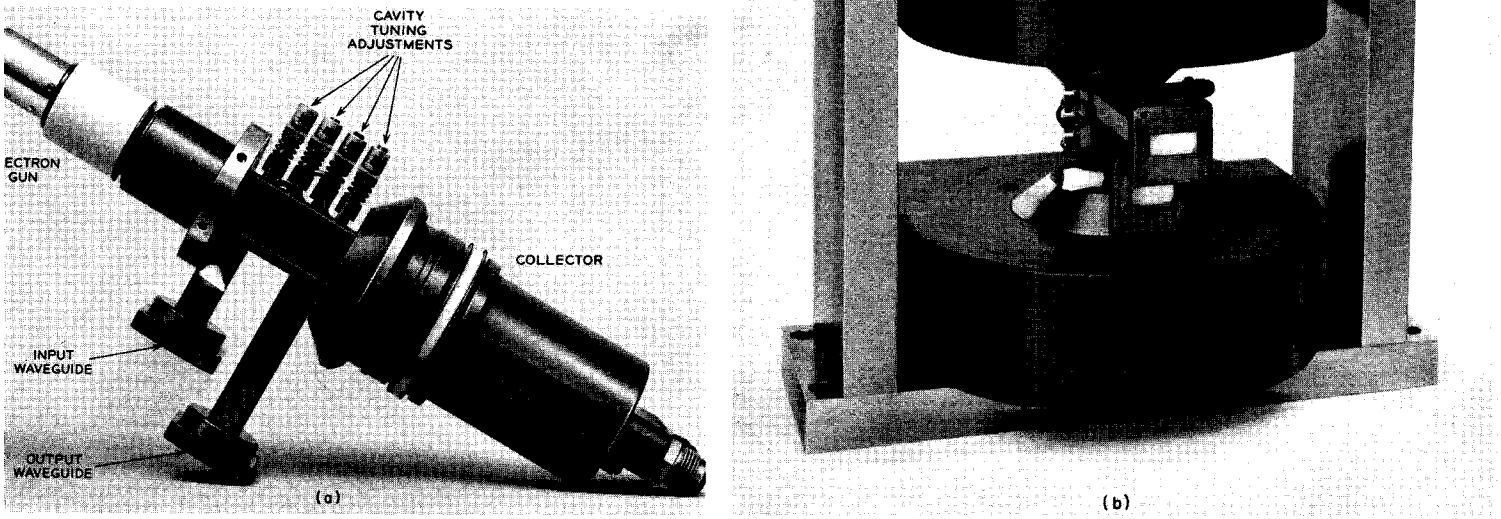

FIG. 9.4-2 VA-849 four-cavity klystron amplifier. (a) The tube without its electromagnet. The overall length of the tube is approximately 45 cm. (b) The VA-849 in place in its electromagnet. (Courtesy of Varian Associates)

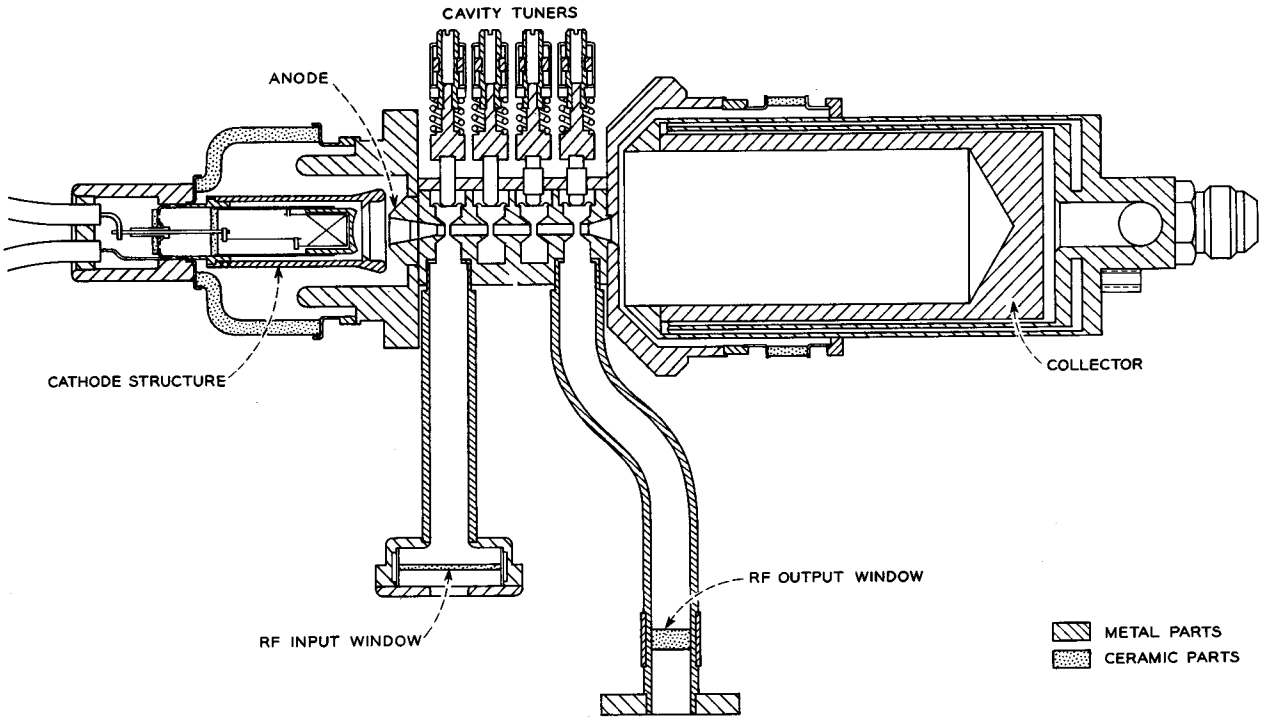

FIG. 9.4-3 Cross-sectional drawing of the VA-849. Each cavity is tuned by deforming a sidewall of the cavity. (Courtesy of Varian Associates)

than a quarter-plasma wavelength, is used in order to increase the bandwidth and efficiency of the tube. The data given in Table 9.4-1 demonstrate

TABLE 9.4-1. VA-849 OPERATING CHARACTERISTICS

Frequency range, Mc	7125–8500
Tuning range, Mc	60
Beam voltage, kv	23
Beam current, amps	2.7
Perveance, amp/volt$^{3/2}$	0.77×10^{-6}
Beam diameter, mm	2.8

	Synchronously Tuned	*Third Cavity Detuned*
Saturated power output, kw	18	24
Drive power, watt	.08	1
Gain, db	54	43
Bandwidth (3 db), Mc	18	30
Electronic efficiency, %	29	38

that judicious staggering of the cavity resonant frequencies not only increases the bandwidth but also increases the electronic efficiency, where electronic efficiency is defined as the ratio of rf output power to the dc beam power. The reason for this increase is beyond the scope of this text, but it is an extremely important attribute of the multicavity klystron amplifier. The collector is operated at the same voltage as the cavities and drift regions.

In summary, klystron amplifiers are characterized by high gain, very good efficiency, and freedom from oscillations. On the other hand, their bandwidths are relatively small. In addition, the phase shift through the tube is directly related to the beam velocity; thus, high regulation and low ripple are required in the beam voltage power supply to avoid undesirable phase-shift variations.

PROBLEMS

9.1 It is proposed to construct a two-cavity klystron amplifier which will amplify a 1-volt, 1000 cps signal. The input signal is applied directly to the grids of the input cavity to modulate a 100 electron volt electron beam. Explain why such a tube would be impracticable.

9.2 A two-cavity klystron is to be designed to operate as a harmonic generator. The distance between cavities may be varied so as to optimize the induced current for the desired harmonic. Calculate the magnitudes of the harmonic currents induced in the output cavity for second, third, and fourth harmonic operation. Compare these values with the magnitude of the fundamental induced current used for

two-cavity amplifier interaction. The cavity gap dimensions remain fixed; the gap transit angle is $\pi/2$ radians for the fundamental frequency.

Ans.: $I_2/I_1 = 0.581$, $I_3/I_1 = 0.248$, $I_4/I_1 = 0$.

9.3 The primary beam current passing through the cavity of a reflex klystron is I_o amps. If the tube is operating in the $1\frac{3}{4}$ mode and generating power at the hot resonant frequency f_o of the cavity (i.e., the resonant frequency when beam loading is included), show that the average amount of charge present in the region between the cavity gap and the repeller is given by $-7I_o/4f_o$.

9.4 The repeller electrode of a particular reflex klystron is planar and parallel to the grids of the resonant cavity, so that the electrons between the gap and the repeller experience a uniform retarding field. Voltages are applied as in Figure 9.2-1. The voltage V_{Ro} is such that the electron transit angle θ_o is equal to $(n + \frac{3}{4})$ 2π.

(a) Show that if an incremental voltage ΔV_{Ro} is added to the voltage V_{Ro}, the incremental change in transit angle is given by

$$\Delta\theta = \theta_o\left(\frac{\Delta\omega}{\omega_o} - \frac{\Delta V_{Ro}}{V_o + V_{Ro}}\right)$$

(b) Using Figure 9.2-4, show that $\Delta\theta$ is also given by

$$\Delta\theta = -2Q_l\frac{\Delta\omega}{\omega_o}$$

(c) Show that if Q_l is large compared with θ_o,

$$\Delta\omega = +\frac{\omega_o}{Q_l}(n + \tfrac{3}{4})\pi\frac{\Delta V_{Ro}}{V_o + V_{Ro}}.$$

9.5 Does the plasma transit angle $\beta_q L$ between cavities vary with frequency? Here L is taken to be the distance between cavities. Explain.

9.6 An electron beam, confined to flow in the z direction by an infinite magnetic field, completely fills a perfectly conducting metal cylinder. $\beta_e b = \beta_e a = 1$. Space-charge waves exist on this beam as given by Equations (9.3-31) and (9.3-33). At a point where the ac component of convection current is zero (i.e., at $\beta_q z = n\pi$), the diameter of the metal cylinder is abruptly doubled. Assume that the dc beam velocity remains unchanged through this discontinuity. At the discontinuity, conservation of kinetic energy dictates continuity of the ac velocity, and the ac convection current is always continuous at a discontinuity where there is no beam interception.

Find the ratios of the maximum values of ac velocity and convection current of the second drift region to the corresponding quantities of the first. Use Figure 9.3-3 to determine the space-charge reduction factors. *Ans.*: 1.0, 0.7.

9.7 A pure slow space-charge wave results in the beam beyond the output cavity when the output gap voltage is given by Equation (9.3-42).

(a) What is the value of output circuit conductance which results in this voltage?
(b) Show that a negative conductance of the same value results in a pure fast space-charge wave beyond the output cavity.

These results demonstrate that a slow space-charge wave is excited by extracting rf energy from an electron beam, whereas a fast space-charge wave is excited by adding rf energy to an electron beam.

9.8 A three-cavity klystron amplifier is designed to operate at a midband frequency of 9 Gc. Assume gridded gaps of 1.27-mm separation and that cavity losses are negligible. The beam voltage is 5 kv, and the beam current is 1 amp. The beam diameter is 5.08 mm, and the space-charge reduction factor R is equal to 0.6.

(a) Show that the midband gain is equal to 69.3 db.
(b) What is the distance between cavity gaps?

9.9 The gain-bandwidth product of an amplifier is defined as the product of the midband voltage gain and the half-power bandwidth. In the case of a klystron amplifier, the voltage gain may be taken as the square root of the power gain.

(a) Obtain an expression for the gain-bandwidth product of two two-cavity klystron amplifiers in series from Equation (9.4-12).
(b) Obtain an expression for the gain-bandwidth product of the three-cavity klystron amplifier from Equation (9.4-17), and compare with the result for part (a).

9.10 Derive an expression for the power gain of a four-cavity klystron amplifier. All cavities are spaced a quarter-plasma wavelength apart. The two intermediate cavities have no external loading, but the input and output cavities are matched to the external circuits for maximum power transfer.

9.11 A two-cavity klystron amplifier is made into an oscillator by feeding back some of the power from the output cavity into the input cavity. The feedback factor (the ratio of input-cavity-gap voltage to output-cavity-gap voltage) is $De^{-i\varphi}$, where D and φ are real numbers varied to change the frequency of oscillation. Neglect any cavity loading caused by the feedback path. The load is matched to the output cavity for maximum power transfer. The spacing between cavities is assumed to be a quarter-plasma wavelength for all frequencies of interest.

(a) Sketch equivalent circuits for both cavities, labeling voltages, currents and impedances in the conventional manner.
(b) Using the space-charge wave equations, find the ratio of the phasors representing the input-gap voltage and the current induced in the output cavity.
(c) From the equivalent circuit and the results of part (b), find the ratio of the phasors representing the two cavity-gap voltages and equate this to the ratio given by the feedback factor.
(d) Taking the real and imaginary parts of the result of part (c), obtain two equations relating ω, φ, and D.
(e) Eliminate D between the latter two equations and obtain φ as a function of ω, ω_q, and the cavity parameters.

REFERENCES

Three references on klystron principles and reflex klystrons are:

9a. K. R. Spangenberg, *Vacuum Tubes*, Chapter 17, McGraw-Hill Book Co., Inc., New York, 1948.
9b. J. C. Slater, *Microwave Electronics*, Chapter 10, D. Van Nostrand Co., Inc., Princeton, N. J., 1950.

9c. W. W. Harman, *Electronic Motion*, Chapter 7, McGraw-Hill Book Co., Inc., New York, 1953.
9d. A. H. W. Beck, "Velocity-Modulated Thermionic Tubes," Cambridge University Press, Cambridge, England, 1948.

Three references on space-charge waves are:

9e. A. H. W. Beck, *Space-Charge Waves and Slow Electromagnetic Waves*, Chapters 4 and 6, Pergamon Press, Inc., New York, 1958.
9f. R. G. E. Hutter, *Beam and Wave Electronics in Microwave Tubes*, Chapter 9, D. Van Nostrand Co., Inc., Princeton N. J., 1960.
9g. W. J. Kleen, "Electronics of Microwave Tubes," Chapter 11, Academic Press, Inc., New York, 1958.

Other references covering specific items discussed in the chapter are:

9.1 E. Jahnke and F. Emde, *Tables of Functions with Formulae and Curves*, Dover Publications, Inc., New York, 1945.
9.2 E. L. Ginzton, *Microwave Measurements*, Chapter 9, McGraw-Hill Book Co., Inc., New York, 1957.
9.3 G. M. Branch and T. G. Mihran, "Plasma Frequency Reduction Factors in Electron Beams," *Trans. IRE* **ED-2**, 3–11, April, 1955.
9.4 S. E. Webber, "Ballistic Analysis of a Two-Cavity Finite Beam Klystron," *Trans. IRE* **ED-5**, 98–108, April, 1958.
9.5 *Reference Data for Radio Engineers*, 4th Ed., International Telephone and Telegraph Corp., p. 242, 1956.
9.6 E. McCune, I. Maltzer, and L. T. Zitelli, "A 20 Kw CW X-Band Klystron Amplifier," *Microwave Journal* **IV**, 74–78, August, 1961.